Journal of Computational and Applied Mathematics 381 (2021) 113012

Contents lists available at ScienceDirect

Journal of Computational and Applied Mathematics

journal homepage: www.elsevier.com/locate/cam

Goal–oriented a posteriori error estimation for Dirichlet boundary control problems

Hamdullah Yücel

Institute of Applied Mathematics, Middle East Technical University, 06800 Ankara, Turkey

ARTICLE INFO

Article history:
Received 27 August 2019
Received in revised form 23 March 2020

Keywords:
Dirichlet boundary optimal control
Local discontinuous Galerkin
Goal–oriented adaptivity
A posteriori error estimate
Convection diffusion equation

ABSTRACT

We study goal-oriented a posteriori error estimates for the numerical approximation of Dirichlet boundary control problem governed by a convection diffusion equation with pointwise control constraints on a two dimensional convex polygonal domain. The local discontinuous Galerkin method is used as a discretization technique since the control variable is involved in a variational form in a natural sense. We derive primal–dual weighted error estimates for the objective functional with an error term representing the mismatch in the complementary system due to the discretization. Numerical examples are presented to illustrate the performance of the proposed estimator.

1. Introduction

Many real-life applications such as the shape optimization of technological devices, air pollution problems, and flow control problems lead to optimization problems governed by partial differential equations (PDEs); see, e.g., [1–3]. In such kind of problems, one is interested in the accurate evaluation of some target quantity, such as the value of the solution of the underlying PDE at some reference point in the domain of interest, a physically relevant quantity such as the drag in airfoil design or, in optimal control, the value of the objective function at the solution of the underlying minimization problem. The complexity of such problems requires special care in order to obtain efficient numerical approximation for the optimization problem. One particular way is the adaptive finite element method with the goal of achieving a desired accuracy in the evaluation of the output quantity of interest, which consists of successive loops of the following sequence:

$$\textbf{SOLVE} \rightarrow \textbf{ESTIMATE} \rightarrow \textbf{MARK} \rightarrow \textbf{REFINE}. \tag{1}$$

The **SOLVE** step stands for the numerical solution of the optimization problem in a finite dimensional space defined on the given mesh. The **ESTIMATE** step is the key point of the adaptive finite element method. In this step, local error indicators are computed in terms of the discrete solution without knowledge of the exact solution. They are essential in designing algorithms for mesh adaptation, which equidistribute the computational effort and optimize the computation. Based on the information of the indicators, the **MARK** step selects a subset of elements subject to refinement. The refinement is then executed in the final step **REFINE** of the adaptive loop.

Nowadays, adaptive mesh refinement based on an a posteriori error estimator, contributed to the pioneer work of Babuška and Rheinboldt [4], has become a standard tool in the finite element codes. Most of the error estimators are based on the L^2–norm or the natural norm with respect to the applied discretization strategy, called as a residual-type a posteriori error estimator, for the optimal control problems; see, e.g., [5–14]. However, the main drawback of conventional error estimates is the dependence of often unknown constants. As a consequence, the error estimator cannot obtain

E-mail address: yucelh@metu.edu.tr.

https://doi.org/10.1016/j.cam.2020.113012
0377-0427/

information concerning the quantity of the error. With regard to applications in the scope of engineering, one can be interested with a quantity of interest instead of the global error estimates. This can be achieved by the concept of goal–oriented error estimates based on the error of goal to the energy estimates by means of auxiliary problems [15], recovery based error estimates [16,17], or the dual-weighted residual method [18]. In this paper, our approach will mainly focus on dual-weighted residual based goal-oriented a posteriori error estimation, as done in [19,20] for pointwise control constrained optimal control problems, and in [21–24] for state constrained optimal control problems.

The dual-weighted residual (DWR) method aims at the economical computation of arbitrary quantities of physical interest by properly adapting the computational mesh. This approach is basically based on the dual problem of the underlying system with the target on the right-hand side. Since the dual solution impacts the weights of the resulting error indicators, the proper choice of the weights is crucial for the effectivity of the adaptation process. In particular, they should measure the influence of a present element on the requested goal quantity of interest. Several techniques for approximation of the dual solution have been developed and proposed in the literature; approximation by a higher-order method, approximation by a higher-order interpolation, approximation by difference quotients, or approximation by local residual problems; we refer to [25–27] and references in therein.

In this work, we study a goal-oriented a posteriori error estimation for Dirichlet boundary control problems governed by a convection diffusion equation:

$$\underset{u\in U^{ad}}{\text{minimize}}\ J(y,u)=\frac{1}{2}\|y-y^d\|^2_{0,\Omega}+\frac{\omega}{2}\|u\|^2_{0,\Gamma} \tag{2}$$

subject to

$$\nabla\cdot(-\epsilon\nabla y+\beta y)+\alpha y = f \qquad \text{in } \Omega, \tag{3a}$$
$$y = u \qquad \text{on } \Gamma, \tag{3b}$$

where Ω is a convex polygonal domain in $\mathbb{R}^2$ with Lipschitz boundary $\Gamma = \partial\Omega$. The velocity field is denoted by $\beta \in \left(W^{1,\infty}(\Omega)\right)^2$. We suppose that it satisfies incompressibility condition, that is, $\nabla\cdot\beta = 0$. The constant coefficients $\epsilon > 0$ and $\alpha > 0$ are corresponding to diffusion and reaction terms, respectively. The regularization parameter ω is a positive constant. For the source function f and the desired state y^d, we assume $f, y^d \in L^2(\Omega)$. Further, the admissible control set U^{ad} is specified by

$$U^{ad} := \{u \in L^2(\Gamma) :\ u^a \le u(x) \le u^b \ \text{ a.e. } x \in \Gamma\}, \tag{4}$$

where u^a and u^b are real numbers. It is well-known that the Dirichlet boundary control problem (2)–(4) is equivalent to the following optimality system:

$$\nabla\cdot(-\epsilon\nabla y+\beta y)+\alpha y = f \qquad \text{in } \Omega, \tag{5a}$$
$$y = u \qquad \text{on } \Gamma, \tag{5b}$$
$$\nabla\cdot(-\epsilon\nabla z-\beta z)+\alpha z = y-y^d \qquad \text{in } \Omega, \tag{5c}$$
$$z = 0 \qquad \text{on } \Gamma, \tag{5d}$$
$$\langle \omega u-\epsilon\frac{\partial z}{\partial \mathbf{n}}, w-u\rangle_{0,\Gamma} \ge 0 \qquad w \in U^{ad}, \tag{5e}$$

where $\mathbf{n}$ is the unit outer normal to Γ. We refer [28,29] and reference therein for derivation of the optimality system (5).

In such kind of problems (2)–(4), the Dirichlet boundary data, i.e., control variable, does not directly enter into standard variational setting. Instead, the governing state equation (3) is understood in the very weak sense, see, e.g., [30–34]. Also, on polyhedral domains, corners cause the normal derivatives of the adjoint $\partial z/\partial\mathbf{n}$ in the optimality system (5) to have limited smoothness. In [35], it is shown that the control variable u vanishes on the corners for problems on a convex polygonal domain, whereas the control may have a pole around the corner for a nonconvex polygon domain. To avoid these difficulties, researchers have proposed various approaches including modified cost functionals in [36–38], approximating the Dirichlet boundary condition with a Robin boundary condition in [39], and a mixed formulation in [40].

This paper concerns a numerical investigation of Dirichlet boundary control problems governed by a convection diffusion equation. Therefore, it may become natural to utilize discontinuous Galerkin methods for the spatial discretization of problems involving strong convection and discontinuities. On the other hand, it is meaningful to use a mixed formulation to avoid the variational difficulty as discussed in [30–34] and dependence on the regularization parameter as done in [39]. Therefore, we employ local discontinuous Galerkin (LDG) method as a discretization technique. The LDG method, one of several discontinuous Galerkin methods, can be considered as a mixed finite element method. As in mixed finite element methods, we rewrite the model problem as a system of first-order equations and discretize it by introducing auxiliary variables. However, auxiliary variables can be eliminated from the equations, which is usually not the case for classical methods. In the LDG method, the local conservativity holds compared to standard finite element methods because the conservation laws are weakly enforced element by element. In order to do that, suitable discrete approximations of the traces of the fluxes on the boundary elements are provided by the so-called numerical fluxes. These numerical fluxes enhance the stability of the method, and hence, the quality of the approximation. This is why the LDG method is strongly

related to stabilized mixed finite elements. The stabilization is associated with the jump of the approximate solution across the element boundaries, see, e.g., [41,42] for details. Moreover, both the approximations to the state y and the corresponding auxiliary variable $\mathbf{q} = \nabla y$ on each element belong to the same space. Therefore, the coding of the LDG method is much simpler than that of the standard mixed methods, especially for high-degree polynomial approximations. Last, the LDG method allows for an easy handling of general meshes since no interelement continuity is required. Hence, it is well-suited for *hp*–adaptivity. We would like to refer to [41,43] for details about discontinuous Galerkin methods. Discontinuous Galerkin methods have also been studied in [12–14,44–46] for optimal control problems due to a better convergence behaviour for optimal control problems exhibiting boundary layers.

In the literature there exist extensive numerical studies for a priori error analysis of elliptic Dirichlet boundary control problems; see, e.g., [31,32,34,35,40,47–51] and references therein. However, there are a few studies for a posteriori error estimation of Dirichlet boundary control problems. Only in [36,37], residual-type a posteriori error analyses were carried out for Dirichlet boundary control governed by an elliptic equation with the control variable defined on an equivalent form of the norm in $H^{\frac{1}{2}}(\Gamma)$. With the present paper we intend to contribute a goal-oriented posteriori error estimation of Dirichlet boundary control problems governed by a convection diffusion equation, considering the control variable in $L^2(\Gamma)$–norm.

We begin, in the next section, by presenting Dirichlet boundary control problem, discretized by the local discontinuous Galerkin method. Section 3 is devoted to derivation of a primal–dual weighted error representation for the objective functional. It is shown that the control constraints yield an error term representing the mismatch in the complementary system due to the discretization. Numerical results are given in Section 4 to show the efficiency of the proposed error estimator. Conclusions and discussions are provided in the last section.

2. Model problem

Throughout the paper we adopt the standard notation $W^{m,p}(\Omega)$ for Sobolev spaces on Ω with norm $\|\cdot\|_{m,p,\Omega}$ and seminorm $|\cdot|_{m,p,\Omega}$ for $m \geq 0$ and $1 \leq p \leq \infty$. We denote $W^{m,2}(\Omega)$ by $H^m(\Omega)$ with norm $\|\cdot\|_{m,\Omega}$ and seminorm $|\cdot|_{m,\Omega}$. It is noted that $H^0(\Omega) = L^2(\Omega)$ and $H_0^1(\Omega) = \{v \in H^1(\Omega) : \ v = 0 \ \text{ on } \ \partial\Omega\}$. The L^2–inner products on $L^2(\Omega)$ and $L^2(\Gamma)$ are defined by

$$(v, w)_{0,\Omega} = \int_\Omega v\, w \ dx \qquad \forall v,\ w \in L^2(\Omega) \quad \text{and} \quad \langle v, w\rangle_{0,\Gamma} = \int_\Gamma v\, w \ ds \qquad \forall v,\ w \in L^2(\Gamma),$$

respectively. In addition, C denotes a generic positive constant independent of the mesh size h and differs in various estimates. Further, the notation $a \lesssim b$ implies that there exists a constant $C > 0$, depending on the shape regularity of triangulation, such that $a \leq C\, b$.

In order to write the LDG scheme for the optimality system (5), we introduce the following auxiliary variables:

$$\mathbf{q} = \epsilon^{\frac{1}{2}} \nabla y, \qquad \mathbf{p} = -\epsilon^{\frac{1}{2}} \nabla z$$

as done by [40] in a mixed formulation of the optimality system. Then, the optimality system (5) can be rewritten as

$$\begin{aligned}
\nabla \cdot (\beta y - \epsilon^{\frac{1}{2}} \mathbf{q}) + \alpha y &= f && \text{in } \Omega, && (6a)\\
\mathbf{q} &= \epsilon^{\frac{1}{2}} \nabla y && \text{in } \Omega, && (6b)\\
y &= u && \text{on } \Gamma, && (6c)\\
\nabla \cdot (\epsilon^{\frac{1}{2}} \mathbf{p} - \beta z) + \alpha z &= y - y^d && \text{in } \Omega, && (6d)\\
\mathbf{p} &= -\epsilon^{\frac{1}{2}} \nabla z && \text{in } \Omega, && (6e)\\
z &= 0 && \text{on } \Gamma, && (6f)\\
\langle \omega u + \epsilon^{\frac{1}{2}} \mathbf{p} \cdot \mathbf{n}, w - u\rangle_\Gamma &\geq 0 && \forall w \in U^{ad}. && (6g)
\end{aligned}$$

Well-posedness and regularity of the optimality system are contained in the following theorem for the convex polygonal domains. The proof of Theorem 2.1 is omitted here since its proof is very similar with the proofs of in [31, Thm. 3.4] for control constrained problem and of in [34, Lemma 2.9] for unconstrained problem.

Theorem 2.1. *Assume that Ω is a bounded convex polygonal domain with Lipschitz boundary Γ. Let $(y, u, z) \in L^2(\Omega) \times L^2(\Gamma) \times H_0^1(\Omega)$ be the solution of optimality system (6). For $f, y^d \in L^2(\Omega)$ we then have*

$$u \in H^{1/2}(\Gamma), \quad y \in H^1(\Omega), \quad \text{and} \quad z \in H^2(\Omega) \cap H_0^1(\Omega). \tag{7}$$

Moreover, for $y^d \in L^{s_*^d}$, $s_*^d > 2$, we have

$$y \in W^{1,s}(\Omega), \quad u \in W^{1-1/s,s}(\Gamma), \quad z \in W^{2,s}(\Omega), \quad 2 \leq s < s_*, \tag{8}$$

where $s_* = \min\left(s_*^d, s_*^\Omega\right)$ with $s_*^\Omega = \frac{2\omega_{max}}{2\omega_{max} - \pi}$, and ω_{max} is the maximum interior angle of the polygonal domain Ω with the condition $\omega_{max} > \pi/2$.

We assume that the domain Ω is polygonal such that the boundary is exactly represented by boundaries of triangles. We denote $\{\mathcal{T}_h\}_h$ as a family of shape-regular simplicial triangulations of Ω in sense of [52]. Each mesh $\mathcal{T}_h$ consists of closed triangles such that $\overline{\Omega} = \bigcup_{K\in\mathcal{T}_h} \overline{K}$ holds. We assume that the mesh is regular in the following sense: for different triangles $K_i, K_j \in \mathcal{T}_h$, $i \neq j$, the intersection $K_i \cap K_j$ is either empty or a vertex or an edge, i.e., hanging nodes are not allowed. The diameter of an element K and the length of an edge E are denoted by h_K and h_E, respectively, and also $h = \max_{K\in\mathcal{T}_h} h_K$.

We split the set of all edges $\mathcal{E}_h$ into the set $\mathcal{E}_h^0$ of interior edges and the set $\mathcal{E}_h^\partial$ of boundary edges so that $\mathcal{E}_h = \mathcal{E}_h^0 \cup \mathcal{E}_h^\partial$. Let $\mathbf{n}$ denote the unit outward normal to Γ. The inflow and outflow parts of Γ are denoted by Γ^- and Γ^+, respectively,

$$\Gamma^- = \{x \in \Gamma \,:\, \beta\cdot\mathbf{n} < 0\}, \quad \Gamma^+ = \{x \in \Gamma \,:\, \beta\cdot\mathbf{n} \geq 0\}.$$

Analogously, the inflow and outflow boundaries of an element $K \in \mathcal{T}_h$ are defined by

$$\partial K^- = \{x \in \partial K \,:\, \beta\cdot\mathbf{n}_K < 0\}, \quad \partial K^+ = \{x \in \partial K \,:\, \beta\cdot\mathbf{n}_K \geq 0\},$$

where $\mathbf{n}_K$ is the unit normal vector on the boundary ∂K of an element K.

Let the edge E be a common edge for two elements K and K^e. For a piecewise continuous scalar function y, there are two traces of y along E, denoted by $y|_E$ from inside K and $y^e|_E$ from inside K^e. The jump and average of y across the edge E are defined by:

$$[\![y]\!] = y|_E\mathbf{n}_K + y^e|_E\mathbf{n}_{K^e}, \quad \{y\} = \frac{1}{2}\big(y|_E + y^e|_E\big),$$

where $\mathbf{n}_K$ (resp. $\mathbf{n}_{K^e}$) denotes the unit outward normal to ∂K (resp. ∂K^e). Similarly, for a piecewise continuous vector field $\mathbf{q}$, the jump and average across an edge E are given by

$$[\![\mathbf{q}]\!] = \mathbf{q}|_E\cdot\mathbf{n}_K + \mathbf{q}^e|_E\cdot\mathbf{n}_{K^e}, \quad \{\mathbf{q}\} = \frac{1}{2}\big(\mathbf{q}|_E + \mathbf{q}^e|_E\big).$$

For a boundary edge $E \in K \cap \partial\Omega$, we set $\{\mathbf{q}\} = \mathbf{q}$ and $[\![y]\!] = y\mathbf{n}$, where $\mathbf{n}$ is the outward normal unit vector on Γ. Note that the jump in y is a vector and the jump in $\mathbf{q}$ is a scalar which only involves the normal components of $\mathbf{q}$.

To obtain weak formulation for the state equation in (6), we multiply it by piecewise smooth test functions v and $\mathbf{r}$, respectively, and integrate by parts over the element $K \in \mathcal{T}_h$

$$(\epsilon^{\frac{1}{2}}\mathbf{q} - \beta y, \nabla v)_{0,K} + (\alpha y, v)_{0,K} - \langle(\epsilon^{\frac{1}{2}}\mathbf{q} - \beta y)\cdot\mathbf{n}, v\rangle_{0,\partial K} = (f, v)_K \qquad v \in V, \tag{9a}$$

$$(\mathbf{q}, \mathbf{r})_{0,K} + (\epsilon^{\frac{1}{2}} y, \nabla\cdot\mathbf{r})_{0,K} = \langle\epsilon^{\frac{1}{2}} y, \mathbf{r}\cdot\mathbf{n}\rangle_{0,\partial K} \quad \mathbf{r} \in \mathbf{W}, \tag{9b}$$

where

$$\mathbf{W} := \left\{\mathbf{w} \in \big(L^2(\Omega)\big)^2 \,:\, \nabla\cdot\mathbf{w}|_K \in L^2(K), \quad \forall K \in \mathcal{T}_h\right\}, \tag{10}$$

$$V := \left\{v \in L^2(\Omega) \,:\, v|_K \in L^2(K), \quad \forall K \in \mathcal{T}_h\right\}. \tag{11}$$

Next, we seek to approximate the state solution $(y, \mathbf{q})$ with functions $(y_h, \mathbf{q}_h)$ in the following finite element spaces $\mathbf{W}_h \times V_h \subset \mathbf{W} \times V$:

$$\mathbf{W}_h = \left\{w \in \big(L^2(\Omega)\big)^2 \,:\, w\,|_K \in \big(\mathbb{S}^1(K)\big)^2, \quad \forall K \in \mathcal{T}_h\right\}, \tag{12a}$$

$$V_h = \left\{v \in L^2(\Omega) \,:\, v\,|_K \in \mathbb{S}^1(K), \quad \forall K \in \mathcal{T}_h\right\}, \tag{12b}$$

$$U_h = \left\{u \in L^2(\Gamma) \,:\, u\,|_E \in \mathbb{S}^1(E), \quad \forall E \in \mathcal{E}_h^\partial\right\}, \tag{12c}$$

where $\mathbb{S}^1(K)$ (resp. $\mathbb{S}^1(E)$) is the local finite element space, which consists of linear polynomials in each element K (resp. on E). For a given element $K \in \mathcal{T}_h$, the restrictions to K of y_h and of each of the components of $\mathbf{q}_h$ belong to the same local space; this renders the coding of these methods considerably simpler than that of the standard mixed methods. It is noted that we also define $U_h^{ad} = U_h \cap U^{ad}$.

For all $(v, \mathbf{r}) \in V_h \times \mathbf{W}_h$ the approximate solution $(y_h, \mathbf{q}_h)$ of the state solution $(y, \mathbf{q})$ satisfies

$$(\epsilon^{\frac{1}{2}}\mathbf{q}_h - \beta y_h, \nabla v)_{0,K} + (\alpha y_h, v)_{0,K} - \langle(\epsilon^{\frac{1}{2}}\widehat{\mathbf{q}}_h - \beta\widetilde{y}_h)\cdot\mathbf{n}, v\rangle_{0,\partial K} = (f_h, v)_K, \tag{13a}$$

$$(\mathbf{q}_h, \mathbf{r})_{0,K} + (\epsilon^{\frac{1}{2}} y_h, \nabla\cdot\mathbf{r})_{0,K} = \langle\epsilon^{\frac{1}{2}}\widehat{y}_h, \mathbf{r}\cdot\mathbf{n}\rangle_{0,\partial K}, \tag{13b}$$

where $\widehat{\mathbf{q}}_h, \widetilde{y}_h, \widehat{y}_h$ denote numerical fluxes. They have to be suitably defined in order to ensure the stability of the method and to enhance its accuracy.

We are now ready to introduce the expressions that define the numerical fluxes. The numerical traces of y associated with the diffusion and convection terms are characterized as

$$\widehat{y}_h = \begin{cases} \{y_h\} + \mathbf{C}_{12}\cdot[\![y_h]\!], & E \in \mathcal{E}_h^0, \\ u_h, & E \in \mathcal{E}_h^\partial, \end{cases} \quad \text{and} \quad \widetilde{y}_h = \begin{cases} u_h, & E \in \Gamma^-, \\ \{y_h\} + \mathbf{D}_{11}\cdot[\![y_h]\!], & E \in \mathcal{E}_h^0, \\ y_h, & E \in \Gamma^+, \end{cases} \tag{14}$$

respectively. We note that the numerical trace of y with respect to convection term is the classical upwinding trace. In addition, the numerical flux $\widehat{\mathbf{q}}_h$ is given by

$$\widehat{\mathbf{q}}_h = \begin{cases} \{\mathbf{q}_h\} + C_{11}[\![y_h]\!] - \mathbf{C}_{12}[\![\mathbf{q}_h]\!], & E \in \mathcal{E}_h^0, \\ \mathbf{q}_h + C_{11}(y_h - u_h)\cdot \mathbf{n}, & E \in \mathcal{E}_h^\partial. \end{cases} \tag{15}$$

It is noted that the auxiliary parameters C_{11}, $\mathbf{C}_{12}$, and $\mathbf{D}_{11}$ depend on $x \in E$, where $E \in \mathcal{E}_h$. In the literature, there exist different choices for these parameters; see, e.g., [14,43,53]. In the numerical implementations, C_{11} is chosen as $C_{11} = 1/h_E$ for each $E \in \mathcal{E}_h$, whereas we take $\mathbf{C}_{12}$ normal to the edges and modulus $1/2$, i.e., $\mathbf{C}_{12}\cdot\mathbf{n}_E = \frac{1}{2}$, and the vector function $\mathbf{D}_{11}$ is given by

$$\mathbf{D}_{11}\cdot\mathbf{n} = \frac{1}{2}\,\mathrm{sign}\big(\mathbf{n}\cdot\beta\big).$$

Let $f_h, y_h^d \in V_h$ denote approximations to the right hand side f and the desired state y^d, respectively. Then, putting the numerical fluxes (14) and (15) into (13) and summing over all elements, we obtain

$$\begin{aligned}
&\sum_{K\in\mathcal{T}_h}\int_K (\epsilon^{\frac{1}{2}}\mathbf{q}_h - \beta y_h)\cdot\nabla v\,dx - \sum_{E\in\mathcal{E}_h^0}\int_E \epsilon^{\frac{1}{2}}\,(\{\mathbf{q}_h\} + C_{11}[\![y_h]\!] - \mathbf{C}_{12}[\![\mathbf{q}_h]\!])\cdot[\![v]\!]\,ds \\
&\quad + \sum_{K\in\mathcal{T}_h}\int_K \alpha y_h\, v\,dx + \sum_{E\in\mathcal{E}_h^0}\int_E \big(\{y_h\} + \mathbf{D}_{11}\cdot[\![y_h]\!]\big)\beta\cdot[\![v]\!]\,ds + \sum_{E\in\Gamma^+}\int_E (\mathbf{n}\cdot\beta) y_h\, v\,ds \\
&\quad - \sum_{E\in\mathcal{E}_h^\partial}\int_E \epsilon^{\frac{1}{2}}\big(\mathbf{q}_h\cdot\mathbf{n} + C_{11}y_h\big)\,v\,ds \\
&\quad = \int_\Omega f_h\, v\,dx - \sum_{E\in\mathcal{E}_h^\partial}\int_E \epsilon^{\frac{1}{2}}\,C_{11}u_h\,v\,ds - \sum_{E\in\Gamma^-}\int_E |\beta\cdot\mathbf{n}|u_h\,v\,ds, \\
&\int_\Omega \mathbf{q}_h\cdot\mathbf{r}\,dx + \sum_{K\in\mathcal{T}_h}\int_K \epsilon^{\frac{1}{2}} y_h\,\nabla\cdot\mathbf{r}\,dx - \sum_{E\in\mathcal{E}_h^0}\int_E \epsilon^{\frac{1}{2}}\big(\{y_h\} + \mathbf{C}_{12}\cdot[\![y_h]\!]\big)[\![\mathbf{r}]\!]\,ds \\
&\quad = \sum_{E\in\mathcal{E}_h^\partial}\int_E \epsilon^{\frac{1}{2}} u_h\,\mathbf{r}\cdot\mathbf{n}\,ds.
\end{aligned}$$

For simplicity, we define the following bi(linear) forms:

$$\begin{aligned}
a(\mathbf{q},\mathbf{r}) &:= \int_\Omega \mathbf{q}\cdot\mathbf{r}\,dx, \\
b(y,\mathbf{r}) &:= \sum_{K\in\mathcal{T}_h}\int_K \epsilon^{\frac{1}{2}} y\,\nabla\cdot\mathbf{r}\,dx - \sum_{E\in\mathcal{E}_h^0}\int_E \epsilon^{\frac{1}{2}}\big(\{y\} + \mathbf{C}_{12}\cdot[\![y]\!]\big)[\![\mathbf{r}]\!]\,ds, \\
c(y,v) &:= \sum_{K\in\mathcal{T}_h}\int_K \big(\alpha y\,v - y\beta\cdot\nabla v\big)\,dx + \sum_{E\in\mathcal{E}_h^0}\int_E \big(\{y\} + \mathbf{D}_{11}\cdot[\![y]\!]\big)\beta\cdot[\![v]\!]\,ds \\
&\quad - \sum_{E\in\mathcal{E}_h^0}\int_E \epsilon^{\frac{1}{2}} C_{11}[\![y]\!]\cdot[\![v]\!]\,ds + \sum_{E\in\Gamma^+}\int_E (\mathbf{n}\cdot\beta) y\,v\,ds - \sum_{E\in\mathcal{E}_h^\partial}\int_E \epsilon^{\frac{1}{2}} C_{11} y\,v\,ds, \\
m_1(u,\mathbf{r}) &:= \sum_{E\in\mathcal{E}_h^\partial}\int_E \epsilon^{\frac{1}{2}} u\,\mathbf{r}\cdot\mathbf{n}\,ds, \\
m_2(u,v) &:= -\sum_{E\in\mathcal{E}_h^\partial}\int_E \epsilon^{\frac{1}{2}} C_{11}u\,v\,ds - \sum_{E\in\Gamma^-}\int_E |\beta\cdot\mathbf{n}|u\,v\,ds, \qquad F(v) := \int_\Omega f_h\,v\,dx.
\end{aligned}$$

By applying integration by parts over the first term in $b(\cdot,\cdot)$, we obtain

$$\begin{aligned}
b(y,\mathbf{r}) &= \sum_{K\in\mathcal{T}_h}\int_K \epsilon^{\frac{1}{2}} y\,\nabla\cdot\mathbf{r}\,dx - \sum_{E\in\mathcal{E}_h^0}\int_E \epsilon^{\frac{1}{2}}\big(\{y\} + \mathbf{C}_{12}\cdot[\![y]\!]\big)[\![\mathbf{r}]\!]\,ds \\
&= -\sum_{K\in\mathcal{T}_h}\int_K \epsilon^{\frac{1}{2}}\nabla y\cdot\mathbf{r}\,dx + \sum_{K\in\mathcal{T}_h}\int_{\partial K} \epsilon^{\frac{1}{2}} y\mathbf{r}\cdot\mathbf{n}\,ds - \sum_{E\in\mathcal{E}_h^0}\int_E \epsilon^{\frac{1}{2}}\big(\{y\} + \mathbf{C}_{12}\cdot[\![y]\!]\big)[\![\mathbf{r}]\!]\,ds.
\end{aligned}$$

Then, by following straightforward computation

$$\sum_{K\in\mathcal{T}_h}\int_{\partial K}\epsilon^{\frac{1}{2}}y\mathbf{r}\cdot\mathbf{n}\,ds=\sum_{E\in\mathcal{E}_h^0\cup\mathcal{E}_h^\partial}\int_E\{\mathbf{r}\}\cdot\left[\!\left[\epsilon^{\frac{1}{2}}y\right]\!\right]ds+\sum_{E\in\mathcal{E}_h^0}\int_E[\![\mathbf{r}]\!]\cdot\left\{\!\left\{\epsilon^{\frac{1}{2}}y\right\}\!\right\}ds$$

we have

$$b(y,\mathbf{r})=-\sum_{K\in\mathcal{T}_h}\int_K\epsilon^{\frac{1}{2}}\nabla y\cdot\mathbf{r}\,dx+\sum_{E\in\mathcal{E}_h^0}\int_E\epsilon^{\frac{1}{2}}\left(\{\mathbf{r}\}-\mathbf{C}_{12}[\![\mathbf{r}]\!]\right)\cdot[\![y]\!]\,ds+\sum_{E\in\mathcal{E}_h^\partial}\int_E\epsilon^{\frac{1}{2}}y\mathbf{r}\cdot\mathbf{n}\,ds.$$

Hence, the LDG approximation of the state equation in (6) reads as

$$a(\mathbf{q}_h,\mathbf{r})+b(y_h,\mathbf{r})=m_1(u_h,\mathbf{r})\qquad\forall\mathbf{r}\in\mathbf{W}_h,\tag{16a}$$

$$-b(v,\mathbf{q}_h)+c(y_h,v)=m_2(u_h,v)+F(v)\qquad\forall v\in V_h.\tag{16b}$$

Employing Lagrange multiplier method, see, e.g., [29], to solve the Dirichlet boundary control problem (2)–(4), we derive the following discrete optimality system:

$$a(\mathbf{q}_h,\mathbf{r})+b(y_h,\mathbf{r})=m_1(u_h,\mathbf{r})\qquad\forall\mathbf{r}\in\mathbf{W}_h,\tag{17a}$$

$$-b(v,\mathbf{q}_h)+c(y_h,v)=m_2(u_h,v)+F(v)\qquad\forall v\in V_h,\tag{17b}$$

$$a(\mathbf{p}_h,\boldsymbol{\psi})-b(z_h,\boldsymbol{\psi})=0\qquad\forall\boldsymbol{\psi}\in\mathbf{W}_h,\tag{17c}$$

$$b(\phi,\mathbf{p}_h)+c(\phi,z_h)=(y_h-y_h^d,\phi)_{0,\Omega}\qquad\forall\phi\in V_h,\tag{17d}$$

$$\langle\omega u_h+\epsilon^{\frac{1}{2}}\mathbf{p}_h\cdot\mathbf{n},w-u_h\rangle_{0,\Gamma}\geq 0\qquad\forall w\in U_h^{ad},\tag{17e}$$

where $\left(y_h,\mathbf{q}_h,z_h,\mathbf{p}_h,u_h\right)\in X_h=V_h\times\mathbf{W}_h\times V_h\times\mathbf{W}_h\times U_h^{ad}$.

By invoking a Lagrange multiplier $\sigma_h\in U_h$ pertinent to the pointwise constraints via

$$\omega u_h+\epsilon^{\frac{1}{2}}\mathbf{p}_h\cdot\mathbf{n}+\sigma_h=0,\tag{18a}$$

$$\sigma_h-\max\{0,\sigma_h+\gamma(u_h-u_h^b)\}+\min\{0,\sigma_h-\gamma(u_h^a-u_h)\}=0,\tag{18b}$$

where $\gamma>0$ is an arbitrary fixed real number and the max- and min-operations are understood in the pointwise sense. The equality (18b) is equivalent to the following pointwise complementary system with $\sigma_h=\sigma_h^b-\sigma_h^a$:

$$\sigma_h^b\geq 0,\qquad u_h-u_h^b\leq 0,\qquad \sigma_h^b\left(u_h-u_h^b\right)=0,\tag{19a}$$

$$\sigma_h^a\geq 0,\qquad u_h^a-u_h\leq 0,\qquad \sigma_h^a\left(u_h^a-u_h\right)=0.\tag{19b}$$

It is well known that (18) enjoys the Newton differentiability property (see, [54]), at least for $\gamma=\omega$. Therefore, we can apply a generalized (semi-smooth) Newton iteration. However, the infinite-dimensional generalized differentiability concept of the max- and min-functions requires a norm gap. In case of boundary controls, it is guaranteed by applying a smooth mapping as done in [55, Remark 4.3]. Due to the structure of the nonsmooth part (18b) the Newton iteration can be expressed in terms of an active set strategy. For any Newton iteration step, the discrete active sets are then determined by

$$\mathcal{A}_{a,h}=\bigcup\{x\in E\mid\ \sigma_h(x)-\gamma(u_h^a(x)-u_h(x))<0,\quad\forall E\in\mathcal{E}_h^\partial\},\tag{20a}$$

$$\mathcal{A}_{b,h}=\bigcup\{x\in E\mid\ \sigma_h(x)+\gamma(u_h(x)-u_h^b(x))>0,\quad\forall E\in\mathcal{E}_h^\partial\},\tag{20b}$$

and the inactive set is $\mathcal{I}_h=\mathcal{E}_h^\partial\backslash\{\mathcal{A}_{a,h}\cup\mathcal{A}_{b,h}\}$. Further, the complementarity conditions in (19) can be rewritten as

$$u_h=u_h^a,\quad\sigma_h^b=0,\quad\sigma_h\leq 0\qquad\text{on }\mathcal{A}_{a,h},\tag{21a}$$

$$u_h=u_h^b,\quad\sigma_h^a=0,\quad\sigma_h\geq 0\qquad\text{on }\mathcal{A}_{b,h},\tag{21b}$$

$$u_h^a<u_h<u^b,\quad\sigma_h^a=\sigma_h^b=0,\quad\sigma_h=0\quad\text{on }\mathcal{I}_h.\tag{21c}$$

One of the issues related to the Dirichlet boundary control problems is the regularity of the solutions, depending on the angles of the domain and the regularity of the given data (see [35, Thm. 3.4]). We refer to [31,34,47] for the regularity of the solutions for general convex polygonal domains and references therein. By following [14], the continuous solution $(y,\mathbf{q},z,\mathbf{p},u)$ also satisfies the following optimality system:

$$a(\mathbf{q},\mathbf{r})+b(y,\mathbf{r})=m_1(u,\mathbf{r})\qquad\forall\mathbf{r}\in\mathbf{W},\tag{22a}$$

$$-b(v,\mathbf{q})+c(y,v)=m_2(u,v)+(f,v)_{0,\Omega}\qquad\forall v\in V,\tag{22b}$$

$$a(\mathbf{p},\boldsymbol{\psi})-b(z,\boldsymbol{\psi})=0\qquad\forall\boldsymbol{\psi}\in\mathbf{W},\tag{22c}$$

$$b(\phi,\mathbf{p})+c(\phi,z)=(y-y^d,\phi)_{0,\Omega}\qquad\forall\phi\in V,\tag{22d}$$

$$\langle\omega u+\epsilon^{\frac{1}{2}}\mathbf{p}\cdot\mathbf{n},w-u\rangle_{0,\Gamma}\geq 0\qquad\forall w\in U^{ad},\tag{22e}$$

where the variational inequality (22e) reads as

$$\omega u + \epsilon^{\frac{1}{2}}\mathbf{p}\cdot\mathbf{n} - \underbrace{\sigma^a + \sigma^b}_{=\sigma} = 0, \tag{23a}$$

$$\sigma^b \geq 0, \qquad u - u^b \leq 0, \qquad \sigma^b\big(u - u^b\big) = 0, \tag{23b}$$

$$\sigma^a \geq 0, \qquad u^a - u \leq 0, \qquad \sigma^a\big(u^a - u\big) = 0. \tag{23c}$$

Then, the continuous active sets are corresponding to

$$\mathcal{A}_a = \{x \in \Gamma :\ \sigma(x) - \gamma(u^a(x) - u(x)) < 0\}, \tag{24a}$$

$$\mathcal{A}_b = \{x \in \Gamma :\ \sigma(x) + \gamma(u(x) - u^b(x)) > 0\}, \tag{24b}$$

and the inactive set is $\mathcal{I} = \Gamma\backslash\{\mathcal{A}_a \cup \mathcal{A}_b\}$. Moreover, the complementarity conditions in (23) are equivalent to

$$u = u^a, \quad \sigma^b = 0, \quad \sigma \leq 0 \qquad \text{a.e. on } \mathcal{A}_a, \tag{25a}$$

$$u = u^b, \quad \sigma^a = 0, \quad \sigma \geq 0 \qquad \text{a.e. on } \mathcal{A}_b, \tag{25b}$$

$$u^a < u < u^b, \quad \sigma^a = \sigma^b = 0, \quad \sigma = 0, \quad \text{a.e. on } \mathcal{I}. \tag{25c}$$

3. Goal–oriented error control

In this section we extend the dual-weighted residual method proposed in [56] to Dirichlet boundary control problem governed by a convection diffusion equation under bilateral box constraints. In this context, the objective functional represents the target quantity in the goal-oriented mesh adaption approach.

We first define the continuous Lagrangian functional $\mathcal{L}(x,\sigma)$ as

$$\begin{aligned}\mathcal{L}(x,\sigma) = {} & J(y,u) + m_1(u,\mathbf{p}) - a(\mathbf{q},\mathbf{p}) - b(y,\mathbf{p}) \\ & + m_2(u,z) + (f,z)_{0,\Omega} + b(z,\mathbf{q}) - c(y,z) \\ & + \big(u - u^b, \sigma^b\big)_{0,\Gamma} + \big(u^a - u, \sigma^a\big)_{0,\Gamma},\end{aligned} \tag{26}$$

where $x = \big(y, \mathbf{q}, z, \mathbf{p}, u\big) \in X = V \times \mathbf{W} \times V \times \mathbf{W} \times U^{ad}$ and $\sigma \in L^2(\Gamma)$. It is noted that

$$\mathcal{L}(x,\sigma) = J(y,u),$$

and for all $\delta x \in X$ it holds that

$$\nabla_x \mathcal{L}(x,\sigma)(\delta x) = 0.$$

Also note that the discrete Lagrangian functional is equivalent to

$$\begin{aligned}\mathcal{L}_h(x_h,\sigma_h) = {} & J_h(y_h,u_h) + m_1(u_h,\mathbf{p}_h) - a(\mathbf{q}_h,\mathbf{p}_h) - b(y_h,\mathbf{p}_h) \\ & + m_2(u_h,z_h) + (f_h,z_h)_{0,\Omega} + b(z_h,\mathbf{q}_h) - c(y_h,z_h) \\ & + \big(u_h - u_h^b, \sigma_h^b\big)_{0,\Gamma} + \big(u_h^a - u_h, \sigma_h^a\big)_{0,\Gamma},\end{aligned} \tag{27}$$

where $x_h = \big(y_h, \mathbf{q}_h, z_h, \mathbf{p}_h, u_h\big) \in X_h = V_h \times \mathbf{W}_h \times V_h \times \mathbf{W}_h$, $\sigma_h \in U_h$ and

$$J_h(y_h,u_h) = \frac{1}{2}\|y_h - y_h^d\|_{0,\Omega}^2 + \frac{\omega}{2}\|u_h\|_{0,\Gamma}^2.$$

Then, we have

$$\mathcal{L}_h(x_h,\sigma_h) = J_h(y_h,u_h),$$

and for all $\delta x_h \in X_h$ it holds that

$$\nabla_x \mathcal{L}_h(x_h,\sigma_h)(\delta x_h) = 0$$

which is obtained by taking $z_h = 0$ on the boundary (5).

Here, the second derivative of $\mathcal{L}$ with respect to x does not depend on x and σ. Therefore, we use $\nabla_{xx}\mathcal{L}(\varphi,\phi)$ instead of $\nabla_{xx}\mathcal{L}(x,\sigma)(\varphi,\phi)$ for notational convenience in the rest of the paper. Similar observations also hold true for the discrete Lagrangian $\mathcal{L}_h$.

Now, we establish a representation for the difference of the continuous and discrete goals in terms of Hessian of the Lagrangian and additional contributions as derived in [19,23].

Theorem 3.1. *Let (x_h, σ_h) and (x, σ) be the solutions of (17) and (22), respectively. Then, the following relation holds*

$$\begin{aligned} J(y,u) - J_h(y_h,u_h) = & -\frac{1}{2}\nabla_{xx}\mathcal{L}(x_h - x, x_h - x) + \left(\sigma^b, u_h - u^b\right)_{0,\Gamma} + \left(\sigma^a, u^a - u_h\right)_{0,\Gamma} \\ & + \frac{1}{2}\|y^d\|^2_{0,\Omega} - \frac{1}{2}\|y_h^d\|^2_{0,\Omega} + \left(y_h^d - y^d, y\right)_{0,\Omega} + \left(f - f_h, z_h\right)_{0,\Omega} \\ & + (y^d - y_h^d, y - y_h)_{0,\Omega}. \end{aligned}$$

Proof. With the help of the following observations at optimal solutions

$$J(y,u) = \mathcal{L}(x,\sigma) \qquad \text{and} \qquad J_h(y_h,u_h) = \mathcal{L}_h(x_h,\sigma_h),$$

Taylor expansion, the definitions in (26) and (27), and the complementary conditions in (19) and (23), we obtain

$$\begin{aligned} J(y,u) - J_h(y_h,u_h) = & \ \mathcal{L}(x,\sigma) - \mathcal{L}_h(x,\sigma_h) - \nabla_x\mathcal{L}_h(x,\sigma_h)(x_h - x) \\ & - \frac{1}{2}\nabla_{xx}\mathcal{L}_h(x_h - x, x_h - x) \\ = & \ J(y,u) - J_h(y,u) + (f - f_h, z)_{0,\Omega} \\ & - \left(u - u_h^b, \sigma_h^b\right)_{0,\Gamma} - \left(u_h^a - u, \sigma_h^a\right)_{0,\Gamma} \\ & - \nabla_x\mathcal{L}_h(x,\sigma_h)(x_h - x) - \frac{1}{2}\nabla_{xx}\mathcal{L}_h(x_h - x, x_h - x) \\ = & \ \frac{1}{2}\|y - y^d\|^2_{0,\Omega} - \frac{1}{2}\|y - y_h^d\|^2_{0,\Omega} + (f - f_h, z)_{0,\Omega} \\ & + (f_h - f, z - z_h)_{0,\Omega} + (y^d - y_h^d, y - y_h)_{0,\Omega} - \nabla_x\mathcal{L}(x,\sigma_h)(x_h - x) \\ & \underbrace{-\left(u - u_h, \sigma_h^b\right) - \left(u_h - u, \sigma_h^a\right)}_{(\sigma_h, u_h - u)} - \frac{1}{2}\nabla_{xx}\mathcal{L}_h(x_h - x, x_h - x). \end{aligned}$$

Note that $x_h \in X_h \subset X$. Then, the expression

$$\nabla_x\mathcal{L}(x,\sigma_h)(x_h - x) = \underbrace{\nabla_x\mathcal{L}(x,\sigma)(x_h - x)}_{=0} + \left(u_h - u, \sigma_h - \sigma\right)$$

yields

$$\begin{aligned} J(y,u) - J_h(y_h,u_h) = & \ \frac{1}{2}\|y - y^d\|^2_{0,\Omega} - \frac{1}{2}\|y - y_h^d\|^2_{0,\Omega} + \left(f - f_h, z_h\right)_{0,\Omega} \\ & + (y^d - y_h^d, y - y_h)_{0,\Omega} + \left(\sigma, u_h - u\right)_{0,\Gamma} - \frac{1}{2}\nabla_{xx}\mathcal{L}_h(x_h - x, x_h - x). \end{aligned}$$

Finally, the complementary condition in (23) produces the desired result. □

Now, we will summarize some known results, which will be needed in the rest of the paper.

- Let $i_h : V \to V_h$ and $I_h : \mathbf{W} \to \mathbf{W}_h$ be the special interpolation operators satisfying (see [57, Chapter III] and [58, Section 3])

$$(y - i_h y, v)_\Omega = 0 \qquad \forall v \in V_h, \tag{28a}$$

$$\left(\nabla\cdot(\mathbf{q} - I_h\mathbf{q}), v\right)_\Omega = 0 \qquad \forall v \in V_h. \tag{28b}$$

  Then, the following approximation estimates hold

$$\|y - i_h y\|_{-s,r,\Omega} \le Ch^{1+s}|y|_{1,r,\Omega}, \qquad s = 0,1, \quad y \in W^{s,r}(\Omega), \tag{29a}$$

$$\|\mathbf{q} - I_h\mathbf{q}\|_{s,r,\Omega} \le Ch^{1-s}|\mathbf{q}|_{1,r,\Omega}, \qquad s = 0,1, \quad \mathbf{q} \in \left(W^{s,r}(\Omega)\right)^2. \tag{29b}$$

- Let $\pi_h : L^2(\Gamma) \to U_h$ be the L^2-projection such that

$$(v - \pi_h v, u_h)_{0,\Gamma} = 0 \qquad \forall u_h \in U_h. \tag{30}$$

  The following approximation property of π_h holds (see [59, Lemma 3.6])

$$|y - \pi_h y|_{0,E} \le Ch^{s-1/2}|y|_{s,K}$$

  for $y \in W^{r,2}(K)$ with $1 \le s \le \min\{2, r\}$. Observing that, for $1/2 < s < 3/2$,

$$u \to \inf_{y|_\Gamma = u} \|y\|_{s,\Omega}$$

is a norm equivalent to $H^{s-1/2}(\Gamma)$, we deduce from above inequality that

$$|u-\pi_h u|_{0,\Gamma} \leq Ch^s |u|_{s,\Gamma} \tag{31}$$

for $u \in H^s(\Gamma)$. Moreover, the following estimate holds (see [59, Equation 3.9])

$$\|\pi_h u\|_{0,\Gamma} \leq \|u\|_{0,\Gamma}. \tag{32}$$

Next, we focus on the evaluation of the Hessian of the Lagrangian in Theorem 3.1 and derive a representation in terms of primal-dual residuals, primal-dual mismatch in complementary, and oscillation terms.

Theorem 3.2. *Let $(x,\sigma) \in X \times L^2(\Gamma)$ and $(x_h,\sigma_h) \in X_h \times U_h$ denote the solutions of (22) and its finite dimensional counterpart (17). Then*

$$J(y,u) - J_h(y_h,u_h) = -r(\iota_h w - w) + \Psi_h + osc_h, \tag{33}$$

where $r(\iota_h w - w)$ stands for the primal–dual weighted residuals

$$\begin{aligned} r(\iota_h w - w) := \frac{1}{2}\Big(& m_1(u_h, I_h\mathbf{p}-\mathbf{p}) - a(\mathbf{q}_h, I_h\mathbf{p}-\mathbf{p}) - b(y_h, I_h\mathbf{p}-\mathbf{p}) \\ & + m_2(u_h, i_h z - z) + (f_h, i_h z - z)_{0,\Omega} + b(i_h z - z, \mathbf{q}_h) - c(y_h, i_h z - z) \\ & - a(\mathbf{p}_h, I_h\mathbf{q}-\mathbf{q}) + b(z_h, I_h\mathbf{q}-\mathbf{q}) \\ & + (y_h - y_h^d, i_h y - y)_{0,\Omega} - b(i_h y - y, \mathbf{p}_h) - c(i_h y - y, z_h) \\ & + (\omega u_h + \epsilon^{\frac{1}{2}}\mathbf{p}_h\cdot\mathbf{n} + \sigma_h, \pi_h u - u)_{0,\Gamma}\Big), \end{aligned} \tag{34}$$

the term Ψ_h represents the primal-dual mismatch in complementary

$$\Psi_h := \frac{1}{2}\left[\left(\sigma_h^b, u_h^b - u\right)_{0,\Gamma} + \left(\sigma_h^a, u - u_h^a\right)_{0,\Gamma} + \left(\sigma^b, u_h - u^b\right)_{0,\Gamma} + \left(\sigma^a, u^a - u_h\right)_{0,\Gamma} \right], \tag{35}$$

and osc_h is given by

$$\begin{aligned} osc_h := & \frac{1}{2}\left(f - f_h, z - z_h\right)_{0,\Omega} - \frac{1}{2}\left(y^d - y_h^d, y - y_h\right)_{0,\Omega} \\ & + \frac{1}{2}\|y^d\|_{0,\Omega}^2 - \frac{1}{2}\|y_h^d\|_{0,\Omega}^2 + \left(y_h^d - y^d, y\right)_{0,\Omega} + \left(f - f_h, z_h\right)_{0,\Omega}. \end{aligned} \tag{36}$$

Note that I_h, i_h, π_h are interpolation operators onto the finite element spaces $\mathbf{W}_h$, V_h, and U_h, respectively, defined in (28) and (30).

Proof. Let $\varphi_h = (\delta y_h, \delta\mathbf{q}_h, \delta z_h, \delta\mathbf{p}_h, \delta u_h) \in X_h \subset X$. It is noted that the second derivative of Lagrangian $\mathcal{L}$ with respect to x does not depend on x and σ. Then, the optimality conditions in continuous and discrete settings and an application of Taylor expansion yield

$$\begin{aligned} 0 &= \nabla_x \mathcal{L}(x,\sigma)(\varphi_h) \\ &= \nabla_x \mathcal{L}(x_h,\sigma)(\varphi_h) + \nabla_{xx}\mathcal{L}(x - x_h, \varphi_h) \\ &= \nabla_x \mathcal{L}(x_h,\sigma_h)(\varphi_h) - (\delta u_h, \sigma_h - \sigma)_{0,\Gamma} + \nabla_{xx}\mathcal{L}(x - x_h, \varphi_h) \\ &= \underbrace{\nabla_x \mathcal{L}_h(x_h,\sigma_h)(\varphi_h)}_{=0} + (f - f_h, \delta z_h)_{0,\Omega} - (y^d - y_h^d, \delta y_h)_{0,\Omega} \\ &\quad + (\delta u_h, \sigma - \sigma_h)_{0,\Gamma} + \nabla_{xx}\mathcal{L}(x - x_h, \varphi_h) \\ &= (\delta u_h, \sigma - \sigma_h)_{0,\Gamma} + \nabla_{xx}\mathcal{L}(x - x_h, \varphi_h) + (f - f_h, \delta z_h)_{0,\Omega} - (y^d - y_h^d, \delta y_h)_{0,\Omega}. \end{aligned} \tag{37}$$

From (37) we have the following relation:

$$\begin{aligned} \nabla_{xx}\mathcal{L}(x_h - x, x_h - x) = & \nabla_{xx}\mathcal{L}(x_h - x, x_h - x + \varphi_h) - (\delta u_h, \sigma - \sigma_h)_{0,\Gamma} \\ & - (f - f_h, \delta z_h)_{0,\Omega} + (y^d - y_h^d, \delta y_h)_{0,\Omega}. \end{aligned} \tag{38}$$

Next, Theorem 3.1 and the equality (38) give us

$$\begin{aligned} J(y,u) - J_h(y_h,u_h) = & \frac{1}{2}\nabla_{xx}\mathcal{L}(x - x_h, x_h - x + \varphi_h) + \frac{1}{2}\left(\delta u_h, \sigma - \sigma_h\right)_{0,\Gamma} \\ & + \frac{1}{2}\left(f - f_h, \delta z_h\right)_{0,\Omega} - \frac{1}{2}\left(y^d - y_h^d, \delta y_h\right)_{0,\Omega} \end{aligned}$$

$$+\left(\sigma^b, u_h-u^b\right)_{0,\Gamma}+\left(\sigma^a, u^a-u_h\right)_{0,\Gamma}$$
$$+\frac{1}{2}\|y^d\|^2_{0,\Omega}-\frac{1}{2}\|y_h^d\|^2_{0,\Omega}+\left(y_h^d-y^d, y\right)_{0,\Omega}+\left(f-f_h, z_h\right)_{0,\Omega}$$
$$+(y^d-y_h^d, y-y_h)_{0,\Omega}.$$

With the help of the following relation:

$$\begin{aligned}\nabla_x\mathcal{L}(x_h,\sigma_h)(x-x_h-\varphi_h) &= \nabla_x\mathcal{L}(x,\sigma_h)(x-x_h-\varphi_h)+\nabla_{xx}\mathcal{L}(x_h-x, x-x_h-\varphi_h)\\ &= \underbrace{\nabla_x\mathcal{L}(x,\sigma)(x-x_h-\varphi_h)}_{=0}+(\sigma_h-\sigma, u-u_h-\delta u_h)_{0,\Gamma}\\ &\quad+\nabla_{xx}\mathcal{L}(x_h-x, x-x_h-\varphi_h),\end{aligned}\tag{39}$$

we obtain

$$\begin{aligned}J(y,u)-J_h(y_h,u_h) &= \frac{1}{2}\nabla_x\mathcal{L}(x_h,\sigma_h)(x-x_h-\varphi_h)-\frac{1}{2}\left(\sigma_h-\sigma, u-u_h-\delta u_h\right)_{0,\Gamma}\\ &\quad+\frac{1}{2}\left(\delta u_h, \sigma-\sigma_h\right)_{0,\Gamma}+\frac{1}{2}\left(f-f_h, \delta z_h\right)_{0,\Omega}-\frac{1}{2}\left(y^d-y_h^d, \delta y_h\right)_{0,\Omega}\\ &\quad+\left(\sigma^b, u_h-u^b\right)_{0,\Gamma}-\underbrace{\left(u-u^b, \sigma^b\right)_{0,\Gamma}}_{=0}+\left(\sigma^a, u^a-u_h\right)_{0,\Gamma}\\ &\quad-\underbrace{\left(u^a-u, \sigma^a\right)_{0,\Gamma}}_{=0}+\frac{1}{2}\|y^d\|^2_{0,\Omega}-\frac{1}{2}\|y_h^d\|^2_{0,\Omega}+\left(y_h^d-y^d, y\right)_{0,\Omega}\\ &\quad+\left(f-f_h, z_h\right)_{0,\Omega}+(y^d-y_h^d, y-y_h)_{0,\Omega}\\ &= -\frac{1}{2}\nabla_x\mathcal{L}_h(x_h,\sigma_h)(x_h-x+\varphi_h)+\frac{1}{2}\left(\sigma_h+\sigma, u_h-u\right)_{0,\Gamma}\\ &\quad+\frac{1}{2}\left(f-f_h, z-z_h\right)_{0,\Omega}-\frac{1}{2}\left(y^d-y_h^d, y-y_h\right)_{0,\Omega}\\ &\quad+\frac{1}{2}\|y^d\|^2_{0,\Omega}-\frac{1}{2}\|y_h^d\|^2_{0,\Omega}+\left(y_h^d-y^d, y\right)_{0,\Omega}+\left(f-f_h, z_h\right)_{0,\Omega}.\end{aligned}$$

Then, choosing $\varphi_h=\left(i_hy-y_h, I_h\mathbf{q}-\mathbf{q}_h, i_hz-z_h, I_h\mathbf{p}-\mathbf{p}_h, \pi_hu-u_h\right)\in X_h$ and using the complementary conditions (19) and (23), we obtain

$$\begin{aligned}&J(y,u)-J_h(y_h,u_h)\\ &= -\frac{1}{2}\nabla_x\mathcal{L}_h(x_h,\sigma_h)\left(i_hy-y, I_h\mathbf{q}-\mathbf{q}, i_hz-z, I_h\mathbf{p}-\mathbf{p}, \pi_hu-u\right)\\ &\quad+\frac{1}{2}\left[\left(\sigma_h^b, u_h^b-u\right)_{0,\Gamma}+\left(\sigma_h^a, u-u_h^a\right)_{0,\Gamma}+\left(\sigma^b, u_h-u^b\right)_{0,\Gamma}+\left(\sigma^a, u^a-u_h\right)_{0,\Gamma}\right]\\ &\quad+\frac{1}{2}\left(f-f_h, z-z_h\right)_{0,\Omega}-\frac{1}{2}\left(y^d-y_h^d, y-y_h\right)_{0,\Omega}\\ &\quad+\frac{1}{2}\|y^d\|^2_{0,\Omega}-\frac{1}{2}\|y_h^d\|^2_{0,\Omega}+\left(y_h^d-y^d, y\right)_{0,\Omega}+\left(f-f_h, z_h\right)_{0,\Omega},\end{aligned}$$

which is the desired result. □

The representation in Theorem 3.2 is not fully a posteriori due to the weights δx_h-x and dependence on the continuous solutions. This fact avoids an immediate numerical implementation of the representation in Theorem 3.2. Now we deduce a fully a posteriori and local indicators from the terms of (33) in Theorem 3.2.

3.1. Primal–dual weighted residuals

First, we concern with an evaluation of the primal-dual weighted residuals $r(\iota_hw-w)$ given in (34).

Theorem 3.3. *The following estimate holds*

$$|r(\iota_h w - w)| \lesssim \frac{1}{2} \sum_{K \in \mathcal{T}_h} \rho_K^y \omega_K^z + \rho_K^{\mathbf{q}} \omega_K^{\mathbf{p}} + \rho_K^z \omega_K^y + \rho_K^{\mathbf{p}} \omega_K^{\mathbf{q}} + \rho_K^u \omega_K^u, \tag{40}$$

where

$$\begin{aligned}
\rho_K^y &= \Bigg(\|f_h - \nabla \cdot (\beta y_h - \epsilon^{\frac{1}{2}} \mathbf{q}_h) - \alpha y_h\|_{0,K}^2 + \sum_{E \in \mathcal{E}_h^0, E \subset \partial K} \|\epsilon^{\frac{1}{2}} [\![\mathbf{q}_h]\!]\|_{0,E}^2 + \|\beta \cdot [\![y_h]\!]\|_{0,E}^2 \\
&\quad + \sum_{E \in \mathcal{E}_h^0, E \subset \partial K} \|\epsilon^{\frac{1}{2}} \mathbf{C}_{12} [\![\mathbf{q}_h]\!]\|_{0,E}^2 + \|(\epsilon^{\frac{1}{2}} C_{11} - \mathbf{D}_{11} \cdot \beta)[\![y_h]\!]\|_{0,E}^2 \\
&\quad + \sum_{E \in \mathcal{E}_h^\partial, E \subset \partial K} \|\epsilon^{\frac{1}{2}} C_{11}(u_h - y_h)\|_{0,E}^2 + \sum_{E \in \Gamma^-, E \subset \partial K} \||\beta \cdot \mathbf{n}|(u_h - y_h)\|_{0,E}^2 \Bigg)^{1/2}, \\
\omega_K^z &= \Bigg(\|i_h z - z\|_{0,K}^2 + \sum_{E \in \mathcal{E}_h^0, E \subset \partial K} \|\{i_h z - z\}\|_{0,E}^2 + \|[\![i_h z - z]\!]\|_{0,E}^2 \\
&\quad + \sum_{E \in \mathcal{E}_h^\partial, E \subset \partial K} \|i_h z - z\|_{0,E}^2 + \sum_{E \in \Gamma^-, E \subset \partial K} \|i_h z - z\|_{0,E}^2 \Bigg)^{1/2}, \\
\rho_K^{\mathbf{q}} &= \Bigg(\|\epsilon^{\frac{1}{2}} \nabla y_h - \mathbf{q}_h\|_{0,K}^2 + \sum_{E \in \mathcal{E}_h^0, E \subset \partial K} \|\epsilon^{\frac{1}{2}} [\![y_h]\!]\|_{0,E}^2 + \|\epsilon^{\frac{1}{2}} \mathbf{C}_{12} \cdot [\![y_h]\!]\|_{0,E} \\
&\quad + \sum_{E \in \mathcal{E}_h^\partial, E \subset \partial K} \|\epsilon^{\frac{1}{2}} (u_h - y_h)\|_{0,E}^2 \Bigg)^{1/2}, \\
\omega_K^{\mathbf{p}} &= \Bigg(\|I_h \mathbf{p} - \mathbf{p}\|_{0,K}^2 + \sum_{E \in \mathcal{E}_h^0, E \subset \partial K} \|\{I_h \mathbf{p} - \mathbf{p}\}\|_{0,E}^2 + \|[\![I_h \mathbf{p} - \mathbf{p}]\!]\|_{0,E}^2 \\
&\quad + \sum_{E \in \mathcal{E}_h^\partial, E \subset \partial K} \|I_h \mathbf{p} - \mathbf{p}\|_{0,E}^2 \Bigg)^{1/2}, \\
\rho_K^z &= \Big(\|y_h - y_h^d - \nabla \cdot (\epsilon^{\frac{1}{2}} \mathbf{p}_h - \beta z_h) - \alpha z_h\|_{0,K}^2 \\
&\quad + \sum_{E \in \mathcal{E}_h^0, E \subset \partial K} \|\epsilon^{\frac{1}{2}} [\![\mathbf{p}_h]\!]\|_{0,E}^2 + \|\beta \cdot [\![z_h]\!]\|_{0,E}^2 \\
&\quad + \sum_{E \in \mathcal{E}_h^0, E \subset \partial K} \|\epsilon^{\frac{1}{2}} \mathbf{C}_{12} [\![\mathbf{p}_h]\!]\|_{0,E}^2 + \|(\epsilon^{\frac{1}{2}} C_{11} - \mathbf{D}_{11} \cdot \beta)[\![z_h]\!]\|_{0,E}^2 \\
&\quad + \sum_{E \in \mathcal{E}_h^\partial, E \subset \partial K} \|\epsilon^{\frac{1}{2}} C_{11} z_h\|_{0,E}^2 + \sum_{E \in \Gamma^+, E \subset \partial K} \||\beta \cdot \mathbf{n}| z_h\|_{0,E}^2 \Big)^{1/2}, \\
\omega_K^y &= \Bigg(\|i_h y - y\|_{0,K}^2 + \sum_{E \in \mathcal{E}_h^0, E \subset \partial K} \|\{i_h y - y\}\|_{0,E}^2 + \|[\![i_h y - y]\!]\|_{0,E}^2 \\
&\quad + \sum_{E \in \mathcal{E}_h^\partial, E \subset \partial K} \|i_h y - y\|_{0,E}^2 + \sum_{E \in \Gamma^+, E \subset \partial K} \|i_h y - y\|_{0,E}^2 \Bigg)^{1/2},
\end{aligned}$$

$$\rho_K^{\mathbf{p}} = \left(\|\epsilon^{\frac{1}{2}} \nabla z_h + \mathbf{p}_h\|_{0,K}^2 + \sum_{E \in \mathcal{E}_h^0, E \subset \partial K} \|\epsilon^{\frac{1}{2}} [\![z_h]\!]\|_{0,E}^2 + \|\epsilon^{\frac{1}{2}} \mathbf{C}_{12} \cdot [\![z_h]\!]\|_{0,E} + \sum_{E \in \mathcal{E}_h^\partial, E \subset \partial K} \|\epsilon^{\frac{1}{2}} z_h\|_{0,E}^2 \right)^{1/2},$$

$$\omega_K^{\mathbf{q}} = \left(\|I_h \mathbf{q} - \mathbf{q}\|_{0,K}^2 + \sum_{E \in \mathcal{E}_h^0, E \subset \partial K} \|\{I_h \mathbf{q} - \mathbf{q}\}\|_{0,E}^2 + \|[\![I_h \mathbf{q} - \mathbf{q}]\!]\|_{0,E}^2 + \sum_{E \in \mathcal{E}_h^\partial, E \subset \partial K} \|I_h \mathbf{q} - \mathbf{q}\|_{0,E}^2 \right)^{1/2},$$

$$\rho_E^u = \sum_{E \in \mathcal{E}_h^\partial} \|\omega u_h + \epsilon^{\frac{1}{2}} \mathbf{p}_h \cdot \mathbf{n} + \sigma_h\|_{0,E}, \qquad \omega_K^u = \sum_{E \in \mathcal{E}_h^\partial} \|\pi_h u - u\|_{0,E}.$$

Proof. First, we consider the following state residual:

$$\begin{aligned} M_y = {} & m_1(u_h, I_h \mathbf{p} - \mathbf{p}) - a(\mathbf{q}_h, I_h \mathbf{p} - \mathbf{p}) - b(y_h, I_h \mathbf{p} - \mathbf{p}) \\ & + m_2(u_h, i_h z - z) + (f_h, i_h z - z)_{0,\Omega} + b(i_h z - z, \mathbf{q}_h) - c(y_h, i_h z - z). \end{aligned}$$

By the definition of the (bi)–linear form and then integration by parts we have

$$\begin{aligned} M_y = {} & \sum_{K \in \mathcal{T}_h} \int_K \big(f_h - \nabla \cdot (\beta y_h - \epsilon^{\frac{1}{2}} \mathbf{q}_h) - \alpha y_h\big)(i_h z - z)\, dx \\ & - \sum_{E \in \mathcal{E}_h^0} \int_E \epsilon^{\frac{1}{2}} \big(\{i_h z - z\} + \mathbf{C}_{12} \cdot [\![i_h z - z]\!]\big)[\![\mathbf{q}_h]\!] \parallel ds \\ & + \sum_{E \in \mathcal{E}_h^0} \int_E \big(\{i_h z - z\} - \mathbf{D}_{11} \cdot [\![i_h z - z]\!]\big)\beta \cdot [\![y_h]\!]\, ds + \sum_{E \in \mathcal{E}_h^0} \int_E \epsilon^{\frac{1}{2}} C_{11} [\![i_h z - z]\!] \cdot [\![y_h]\!]\, ds \\ & + \sum_{E \in \mathcal{E}_h^\partial} \int_E \epsilon^{\frac{1}{2}} C_{11} (y_h - u_h)(i_h z - z)\, ds + \sum_{E \in \Gamma^-} \int_E |\beta \cdot \mathbf{n}| (y_h - u_h)(i_h z - z)\, ds \\ & + \sum_{K \in \mathcal{T}_h} \int_K \big(\epsilon^{\frac{1}{2}} \nabla y_h - \mathbf{q}_h\big)(I_h \mathbf{p} - \mathbf{p})\, dx \\ & - \sum_{E \in \mathcal{E}_h^0} \int_E \epsilon^{\frac{1}{2}} \big(\{I_h \mathbf{p} - \mathbf{p}\} - \mathbf{C}_{12} [\![I_h \mathbf{p} - \mathbf{p}]\!]\big)[\![y_h]\!]\, ds + \sum_{E \in \mathcal{E}_h^\partial} \int_E \epsilon^{\frac{1}{2}} (u_h - y_h)(I_h \mathbf{p} - \mathbf{p})\, ds. \end{aligned}$$

Then, Cauchy–Schwarz inequality and Young's inequality yield

$$\begin{aligned} M_y \le {} & \sum_{K \in \mathcal{T}_h} \|f_h - \nabla \cdot (\beta y_h - \epsilon^{\frac{1}{2}} \mathbf{q}_h) - \alpha y_h\|_{0,K} \|i_h z - z\|_{0,K} \\ & + \sum_{E \in \mathcal{E}_h^0} \Big(\|\epsilon^{\frac{1}{2}} [\![\mathbf{q}_h]\!]\|_{0,E} + \|\beta \cdot [\![y_h]\!]\|_{0,E} \Big) \|\{i_h z - z\}\|_{0,E} \\ & + \sum_{E \in \mathcal{E}_h^0} \Big(\|\mathbf{C}_{12} \epsilon^{\frac{1}{2}} [\![\mathbf{q}_h]\!]\|_{0,E} + \|(\epsilon^{\frac{1}{2}} C_{11} - \mathbf{D}_{11} \cdot \beta)[\![y_h]\!]\|_{0,E} \Big) \|[\![i_h z - z]\!]\|_{0,E} \\ & + \sum_{E \in \mathcal{E}_h^\partial} \epsilon^{\frac{1}{2}} C_{11} \|u_h - y_h\|_{0,E} \|i_h z - z\|_{0,E} + \sum_{E \in \Gamma^-} |\beta \cdot \mathbf{n}| \|u_h - y_h\|_{0,E} \|i_h z - z\|_{0,E} \\ & + \sum_{K \in \mathcal{T}_h} \|\epsilon^{\frac{1}{2}} \nabla y_h - \mathbf{q}_h\|_{0,K} \|I_h \mathbf{p} - \mathbf{p}\|_{0,K} \end{aligned}$$

$$+ \sum_{E\in\mathcal{E}_h^0} \|\epsilon^{\frac{1}{2}}[\![y_h]\!]\|_{0,E} h \|\{I_h\mathbf{p}-\mathbf{p}\}\|_{0,E} + \|\mathbf{C}_{12}\epsilon^{\frac{1}{2}}[\![y_h]\!]\|_{0,E}\|[\![I_h\mathbf{p}-\mathbf{p}]\!]\|_{0,E}$$
$$+ \sum_{E\in\mathcal{E}_h^\partial} \epsilon^{\frac{1}{2}}\|u_h-y_h\|_{0,E}\|I_h\mathbf{p}-\mathbf{p}\|_{0,E} \lesssim \sum_{K\in\mathcal{T}_h} \rho_K^y\omega_K^z + \rho_K^{\mathbf{q}}\omega_K^{\mathbf{p}}.$$

Analogously, we derive the estimates for the adjoint and the control. □

In the a posteriori error estimates (40), the residuals of the state system are weighted by the adjoint variables, in turn, those of the adjoint system by the state variables. In this way, the proposed estimator exhibits particular sensitivities of the optimization problem. We note that the estimates in (40) still depend on the continuous solutions. To overcome this difficulty, we replace y, $\mathbf{q}$, z, $\mathbf{p}$, u by y_h, $\mathbf{q}_h$, z_h, $\mathbf{p}_h$, u_h. On the other hand, we use an average technique for the interpolation functions $\zeta \in \{i_h y, I_h\mathbf{q}, i_h z, I_h\mathbf{p}\}$ in the element $K \in \mathcal{T}_h$

$$\widetilde{\zeta}|_K := \mathrm{card}(\mathcal{N}(K))^{-1} \sum_{K\in\mathcal{N}(K)} \zeta_K, \tag{41}$$

where

$$\mathcal{N}(K) := \{K\} \cup \{K' \mid K\cap K' \neq \emptyset\}.$$

Note that the contributions coming from the edges in (40) are eliminated with the help of the trace inequality, see, e.g., [60, Section 1.6]. Further, typically $\|\omega u_h + \epsilon^{\frac{1}{2}}\mathbf{p}_h\cdot\mathbf{n} + \sigma_h\|_{0,E}$ is small, or, when the same ansatz is used for discretization, it is even zero.

Hence, a posteriori estimate for the primal–dual weighted residuals becomes

$$|r(\iota_h w - w)| \lesssim \frac{1}{2}\sum_{K\in\mathcal{T}_h} \rho_K^y\widetilde{\omega}_K^z + \rho_K^{\mathbf{q}}\widetilde{\omega}_K^{\mathbf{p}} + \rho_K^z\widetilde{\omega}_K^y + \rho_K^{\mathbf{p}}\widetilde{\omega}_K^{\mathbf{q}}, \tag{42}$$

where $\widetilde{\omega}_K^\nu$ with $\nu \in \{z, \mathbf{p}, y, \mathbf{q}\}$ are approximations to ω_K^ν, obtained by (41).

3.2. Primal–dual mismatch in complementary

Now we concentrate the errors coming from complementary slackness (35). It can be written as

$$\Psi_h := \frac{1}{2}\left[\left(\sigma_h^b, u_h^b - u\right)_{0,\Gamma} + \left(\sigma_h^a, u - u_h^a\right)_{0,\Gamma} + \left(\sigma^b, u_h - u^b\right)_{0,\Gamma} + \left(\sigma^a, u^a - u_h\right)_{0,\Gamma}\right]. \tag{43}$$

This term cannot be immediately handled due to continuous unknowns u, σ^b, and σ^a. Using discrete and continuous complementary conditions in (21) and (25), we derive the following estimates on the respective sets:

$$\begin{aligned}
\Psi_h(\mathcal{I}\cap\mathcal{I}_h) &= 0 := \psi^1,\\
\Psi_h(\mathcal{I}\cap\mathcal{A}_{a,h}) &= \frac{1}{2}(\sigma_h^a, u-u_h^a)_{0,\mathcal{I}\cap\mathcal{A}_{a,h}} = \frac{1}{2}(\sigma_h^a, -u_h^a - \frac{\sqrt{\epsilon}}{\omega}\mathbf{p}\cdot\mathbf{n})_{0,\mathcal{I}\cap\mathcal{A}_{a,h}}\\
&\le \frac{1}{2}\|\sigma_h^a\|_{0,\mathcal{I}\cap\mathcal{A}_{a,h}}\left(\|u_h^a + \frac{\sqrt{\epsilon}}{\omega}\mathbf{p}_h\cdot\mathbf{n}\|_{0,\mathcal{I}\cap\mathcal{A}_{a,h}} + \frac{\sqrt{\epsilon}}{\omega}\|(\mathbf{p}_h-\mathbf{p})\cdot\mathbf{n}\|_{0,\mathcal{I}\cap\mathcal{A}_{a,h}}\right)\\
&:= \psi^2,\\
\Psi_h(\mathcal{I}\cap\mathcal{A}_{b,h}) &= \frac{1}{2}(\sigma_h^b, u_h^b-u)_{0,\mathcal{I}\cap\mathcal{A}_{b,h}} = \frac{1}{2}(\sigma_h^b, u_h^b + \frac{\sqrt{\epsilon}}{\omega}\mathbf{p}\cdot\mathbf{n})_{0,\mathcal{I}\cap\mathcal{A}_{b,h}}\\
&\le \frac{1}{2}\|\sigma_h^b\|_{0,\mathcal{I}\cap\mathcal{A}_{b,h}}\left(\|u_h^b + \frac{\sqrt{\epsilon}}{\omega}\mathbf{p}_h\cdot\mathbf{n}\|_{0,\mathcal{I}\cap\mathcal{A}_{b,h}} + \frac{\sqrt{\epsilon}}{\omega}\|(\mathbf{p}-\mathbf{p}_h)\cdot\mathbf{n}\|_{0,\mathcal{I}\cap\mathcal{A}_{b,h}}\right)\\
&:= \psi^3,\\
\Psi_h(\mathcal{A}_a\cap\mathcal{I}_h) &= \frac{1}{2}(\sigma^a, u^a-u_h)_{0,\mathcal{A}_a\cap\mathcal{I}_h}\\
&\le \frac{\omega}{2}(u-u_h, u-u_h)_{0,\mathcal{A}_a\cap\mathcal{I}_h} + \frac{\sqrt{\epsilon}}{2}\left((\mathbf{p}-\mathbf{p}_h)\cdot\mathbf{n}, u-u_h\right)_{0,\mathcal{A}_a\cap\mathcal{I}_h}\\
&\le \frac{1}{2}\|u^a-u_h\|_{0,\mathcal{A}_a\cap\mathcal{I}_h}\left(\omega\|u^a-u_h\|_{0,\mathcal{A}_a\cap\mathcal{I}_h} + \sqrt{\epsilon}\|(\mathbf{p}-\mathbf{p}_h)\cdot\mathbf{n}\|_{0,\mathcal{A}_a\cap\mathcal{I}_h}\right)\\
&:= \psi^4,
\end{aligned}$$

$$
\begin{aligned}
\Psi_h(\mathcal{A}_a \cap \mathcal{A}_{b,h}) &= \frac{1}{2}(\sigma_h^b, u_h^b - u)_{0,\mathcal{A}_a\cap\mathcal{A}_{b,h}} + \frac{1}{2}(\sigma^a, u^a - u_h)_{0,\mathcal{A}_a\cap\mathcal{A}_{b,h}} \\
&= \frac{1}{2}(\sigma_h^b, u_h - u)_{0,\mathcal{A}_a\cap\mathcal{A}_{b,h}} + \frac{\omega}{2}(u - u_h, u - u_h)_{0,\mathcal{A}_a\cap\mathcal{A}_{b,h}} \\
&\quad + \frac{\sqrt{\epsilon}}{2}((\mathbf{p} - \mathbf{p}_h)\cdot\mathbf{n}, u - u_h)_{0,\mathcal{A}_a\cap\mathcal{A}_{b,h}} \\
&\leq \frac{1}{2}\|u_h - u^a\|_{0,\mathcal{A}_a\cap\mathcal{A}_{b,h}} \\
&\quad \times \left(\|\sigma_h^b\|_{0,\mathcal{A}_a\cap\mathcal{A}_{b,h}} + \omega\|u^a - u_h\|_{0,\mathcal{A}_a\cap\mathcal{A}_{b,h}} + \sqrt{\epsilon}\|(\mathbf{p} - \mathbf{p}_h)\cdot\mathbf{n}\|_{0,\mathcal{A}_a\cap\mathcal{A}_{b,h}}\right) \\
&:= \psi^5, \\
\Psi_h(\mathcal{A}_a \cap \mathcal{A}_{a,h}) &= \frac{1}{2}(\sigma_h^a, u - u_h^a)_{0,\mathcal{A}_a\cap\mathcal{A}_{a,h}} + \frac{1}{2}(\sigma^a, u^a - u_h)_{0,\mathcal{A}_a\cap\mathcal{A}_{a,h}} \\
&= \frac{1}{2}(\sigma_h^a, u - u_h)_{0,\mathcal{A}_a\cap\mathcal{A}_{a,h}} \\
&\quad + \frac{1}{2}\left(\omega u + \sqrt{\epsilon}\mathbf{p}\cdot\mathbf{n} - \omega u_h - \sqrt{\epsilon}\mathbf{p}_h\cdot\mathbf{n} + \sigma_h^a, u - u_h\right)_{0,\mathcal{A}_a\cap\mathcal{A}_{a,h}} \\
&\leq \|u^a - u_h\|_{0,\mathcal{A}_a\cap\mathcal{A}_{a,h}} \\
&\quad \times \left(\|\sigma_h^a\|_{0,\mathcal{A}_a\cap\mathcal{A}_{b,h}} + \frac{\omega}{2}\|u^a - u_h\|_{0,\mathcal{A}_a\cap\mathcal{A}_{a,h}} + \frac{\sqrt{\epsilon}}{2}\|(\mathbf{p} - \mathbf{p}_h)\cdot\mathbf{n}\|_{0,\mathcal{A}_a\cap\mathcal{A}_{a,h}}\right) \\
&:= \psi^6, \\
\Psi_h(\mathcal{A}_b \cap \mathcal{I}_h) &= \frac{1}{2}(\sigma^b, u_h - u^b)_{0,\mathcal{A}_b\cap\mathcal{I}_h} \\
&= \frac{\omega}{2}(u_h - u, u_h - u)_{0,\mathcal{A}_b\cap\mathcal{I}_h} + \frac{\sqrt{\epsilon}}{2}((\mathbf{p}_h - \mathbf{p})\cdot\mathbf{n}, u_h - u)_{0,\mathcal{A}_b\cap\mathcal{I}_h} \\
&\leq \frac{1}{2}\|u_h - u^b\|_{0,\mathcal{A}_b\cap\mathcal{I}_h}\left(\omega\|u_h - u^b\|_{0,\mathcal{A}_b\cap\mathcal{I}_h} + \sqrt{\epsilon}\|(\mathbf{p}_h - \mathbf{p})\cdot\mathbf{n}\|_{0,\mathcal{A}_b\cap\mathcal{I}_h}\right) \\
&:= \psi^7, \\
\Psi_h(\mathcal{A}_b \cap \mathcal{A}_{a,h}) &= \frac{1}{2}(\sigma_h^a, u - u_h^a)_{0,\mathcal{A}_b\cap\mathcal{A}_{a,h}} + \frac{1}{2}(\sigma^b, u_h - u^b)_{0,\mathcal{A}_b\cap\mathcal{A}_{a,h}} \\
&\leq \frac{1}{2}(\sigma_h^a, u - u_h)_{0,\mathcal{A}_b\cap\mathcal{A}_{a,h}} + \frac{\omega}{2}(u - u_h, u - u_h)_{0,\mathcal{A}_b\cap\mathcal{A}_{a,h}} \\
&\quad + \frac{\sqrt{\epsilon}}{2}((\mathbf{p} - \mathbf{p}_h)\cdot\mathbf{n}, u - u_h)_{0,\mathcal{A}_b\cap\mathcal{A}_{a,h}} + \frac{1}{2}(\sigma_h^a, u - u_h)_{0,\mathcal{A}_b\cap\mathcal{A}_{a,h}} \\
&\leq \|u^b - u_h\|_{0,\mathcal{A}_b\cap\mathcal{A}_{a,h}} \\
&\quad \times \left(\|\sigma_h^a\|_{0,\mathcal{A}_b\cap\mathcal{A}_{a,h}} + \frac{\omega}{2}\|u^b - u_h\|_{0,\mathcal{A}_b\cap\mathcal{A}_{a,h}} + \frac{\sqrt{\epsilon}}{2}\|(\mathbf{p} - \mathbf{p}_h)\cdot\mathbf{n}\|_{0,\mathcal{A}_b\cap\mathcal{A}_{a,h}}\right) \\
&:= \psi^8, \\
\Psi_h(\mathcal{A}_b \cap \mathcal{A}_{b,h}) &= \frac{1}{2}(\sigma_h^b, u_h^b - u)_{0,\mathcal{A}_b\cap\mathcal{A}_{b,h}} + \frac{1}{2}(\sigma^b, u_h - u^b)_{0,\mathcal{A}_b\cap\mathcal{A}_{b,h}} \\
&\leq \|u_h - u^b\|_{0,\mathcal{A}_a\cap\mathcal{A}_{b,h}} \\
&\quad \times \left(\|\sigma_h^b\|_{0,\mathcal{A}_b\cap\mathcal{A}_{b,h}} + \frac{\omega}{2}\|u_h - u^b\|_{0,\mathcal{A}_a\cap\mathcal{A}_{b,h}} + \frac{\sqrt{\epsilon}}{2}\|(\mathbf{p}_h - \mathbf{p})\cdot\mathbf{n}\|_{0,\mathcal{A}_b\cap\mathcal{A}_{b,h}}\right) \\
&:= \psi^9.
\end{aligned}
$$

Hence, we obtain the following estimate for the primal-dual mismatch in complementary

$$
|\Psi(\Omega)| \leq \sum_{i=1}^{9} |\psi^i| := \psi. \tag{45}
$$

The estimates in (45) are computable a posteriori except $\|(\mathbf{p}-\mathbf{p}_h)\cdot\mathbf{n}\|_{0,S}$ for any set S. The continuous solutions are approximated as follows

$$\widetilde{\zeta}|_E := \operatorname{card}(\mathcal{N}(E))^{-1}\sum_{E\in\mathcal{N}(E)}\zeta_E, \tag{46}$$

where

$$\mathcal{N}(E) := \{E\}\cup\{E' \mid E\cap E'\neq\emptyset\}.$$

However, the estimates in (45) are still not fully a posteriori due to the active or inactive set in continuous setting. By following the steps in [9, Section 3.3], we can derive estimates continuous active or inactive sets by

$$\chi_h^{\mathcal{A}_a} = 1-\frac{u_h-u^a}{\gamma h^r+u_h-u^a},\quad \chi_h^{\mathcal{A}_b} = 1-\frac{u^b-u_h}{\gamma h^r+u^b-u_h},\quad \chi_h^{\mathcal{I}} = 1-\chi_h^{\mathcal{A}_a}-\chi_h^{\mathcal{A}_b},$$

where γ denotes some positive constant and $r>0$ is fixed. Note that $\chi_h^{\mathcal{A}_a}=1$ in $\mathcal{A}_{a,h}$ and $\chi_h^{\mathcal{A}_b}=1$ in $\mathcal{A}_{b,h}$.

Let $\chi(S)$ denote the characteristic function of a set $S\subset\Omega$. For instance, assume that $E\subset\mathcal{A}_a$. Then

$$\|\chi(\mathcal{A}_a)-\chi_h^{\mathcal{A}_a}\|_{0,E} = \left\|\frac{u_h-u^a}{\gamma h^r+u_h-u^a}\right\|_{0,E} \le \min\{1,\gamma^{-1}h^{-r}\|u-u_h\|_{0,E}\},$$

which tends to zero whenever $\|u-u_h\|_{0,E}=\mathcal{O}(h^q)$ with $q>r$. If $E\not\subset\mathcal{A}_a$, then we have two cases:

(i) If $u_h-u^a>\gamma h^{\mu r}$ for some $0\le\mu<1$, then

$$\|\chi(\mathcal{A}_a)-\chi_h^{\mathcal{A}_a}\|_{0,E} = \left\|\frac{\gamma h^r}{\gamma h^r+u_h-u^a}\right\|_{0,E} \le h^{(1-\mu)r}\to 0 \text{ as } h\to 0.$$

(ii) If $u_h-u^a\le\gamma h^{\mu r}$ for some $0\le\mu<1$, then the measure of this set tends to zero as $h\to 0$.

In analogues way, we can find approximations for the sets $\mathcal{A}_b$ and $\mathcal{I}$. Now, we have the following approximation, for instance $S=\mathcal{A}_a\cap\mathcal{I}_h$:

$$\chi(S)\approx\chi_h^{\mathcal{A}_a}\chi(\mathcal{I}_h) =: \chi_h^S.$$

We then use

$$\|\chi_h^S(u_h-u^a)\|_{0,\Omega}\quad\text{instead of}\quad\|u_h-u^a\|_{0,\mathcal{A}_a\cap\mathcal{I}_h},$$

and analogously for other terms in (45). Consequently, we obtain an a posteriori estimate for the primal–dual mismatch in complementary

$$|\Psi(\Omega)|\lesssim\sum_{i=1}^{9}|\widehat{\psi}^i| := |\widehat{\Psi}(\Omega)|. \tag{47}$$

3.3. Primal-dual weighted data oscillations

Last we consider the data oscillation term in (36)

$$\begin{aligned}\operatorname{osc}_h :=\ & \frac{1}{2}\big(f-f_h,z-z_h\big)_{0,\Omega}-\frac{1}{2}\big(y^d-y_h^d,y-y_h\big)_{0,\Omega}\\ &+\frac{1}{2}\|y^d\|_{0,\Omega}^2-\frac{1}{2}\|y_h^d\|_{0,\Omega}^2+\big(y_h^d-y^d,y\big)_{0,\Omega}+\big(f-f_h,z_h\big)_{0,\Omega},\end{aligned} \tag{48}$$

can be estimated by means of

$$\begin{aligned}\widehat{\operatorname{osc}}_h :=\ & \sum_{K\in\mathcal{T}_h}\Big(\frac{1}{2}\|f-f_h\|_{0,K}\|\widetilde{z}_h-z_h\|_{0,K}+\frac{1}{2}\|y^d-y_h^d\|_{0,K}\|\widetilde{y}_h-y_h\|_{0,K}\\ &+\frac{1}{2}\|y^d\|_{0,K}^2-\frac{1}{2}\|y_h^d\|_{0,K}^2+\|y_h^d-y^d\|_{0,K}\|\widetilde{y}_h\|_{0,K}+\|f-f_h\|_{0,K}\|z_h\|_{0,K}\Big),\end{aligned}$$

where $\widetilde{y}_h,\widetilde{z}_h$ are defined in the same way as done in (41).

4. Numerical experiments

We first give a brief overview of the adaptive finite element method (AFEM) in Section 4.1. Then, we establish an optimization algorithm on every adaptive refinement level in Section 4.2. Last, Section 4.3 contains some numerical results to show the efficiency of the derived estimator in Section 3.

4.1. The adaptive loop

An adaptive procedure based on the goal-oriented a posteriori error estimators for the LDG discretization of the optimization problem (2)–(4) consists of successive loops of the sequence given in (1). The mesh adaption process is guided iteratively by local indicators relying on the solutions of the considered on the current mesh. The Algorithm 1 repeats the adaptive procedure until a given complexity #vertices, i.e., the number of vertices.

Algorithm 1 AFEM Algorithm

Input: Triangulation $\mathcal{T}_h$, data f, y^d, u^a, u^b, complexity #dof, bulk parameter θ.
loop
  $(y_h, \mathbf{p}_h, z_h, \mathbf{q}_h, u_h, \sigma_h)$= **solve**$(\mathcal{T}_h, u_h, f, y^d, u^a, u^b)$
  η = **estimate**$(\mathcal{T}_h, y_h, \mathbf{p}_h, z_h, \mathbf{q}_h, u_h, \sigma_h, f, y^d, u^a, u^b)$
  if |#dof$(\mathcal{T}_h)$|> #vertices **then**
    return $(\mathcal{T}_h, y_h, \mathbf{p}_h, z_h, \mathbf{q}_h, u_h, \sigma_h)$
  end if
  $\mathcal{M}_h$=**mark**$(\mathcal{T}_h, \eta, \theta)$
  $\mathcal{T}_h$=**refine**$(\mathcal{T}_h, \mathcal{M}_h)$
end loop

The **SOLVE** step (subroutine **solve**) is the numerical solution of the optimal control problem with respect to the given triangulation $\mathcal{T}_h$ using the LDG discretization and the primal-dual active set (PDAS) algorithm as a semi-smooth Newton step, see, e.g., [61]. The **ESTIMATE** step (subroutine **estimate**) requires the computation of the estimates for the weighted dual residuals, the primal-dual mismatch complementary, and the data oscillations, derived in Section 3. We use a bulk criterion in the **MARK** step (subroutine **mark**) to specify the elements in $\mathcal{T}_h$ by using the a posteriori error estimator and by choosing subsets $\mathcal{M}_K \subset \mathcal{T}_h$ such that the bulk criterion is satisfied for a given marking parameter Θ with $0 < \Theta < 1$:

$$\Theta \sum_{K\in\mathcal{T}_h} \eta_K \leq \sum_{K\in\mathcal{M}_K} \eta_K, \tag{49}$$

where η_K is the a posteriori error estimator derived in Section 3. Bigger values for the parameter Θ will result in more refinement of triangles in one loop, whereas smaller Θ will result in a more optimal grid but more refinement loops. Finally, in the **REFINE** step (subroutine **refine**), the marked elements are refined by longest edge bisection, whereas the elements of the marked edges are refined by bisection strategy.

Algorithm 2 Active Set Algorithm

Input: Given the parameter γ.
Set $k = 0$.
Set initial values for u_h^0, $\sigma_{a,h}^0$, and $\sigma_{b,h}^0$.
Calculate indices of the initial active sets $\mathcal{A}_{a,h}^0$, $\mathcal{A}_{b,h}^0$, and the inactive set $\mathcal{I}_h^0$.
for $k = 1, 2, \ldots$ **do**
  Solve (50) for $\mathcal{Y}_h^k$, u_h^k, $\mathcal{Z}_h^k$, $\sigma_{a,h}^k$, and $\sigma_{b,h}^k$.
  Calculate indices of active sets $\mathcal{A}_{a,h}^k$, $\mathcal{A}_{b,h}^k$, and inactive set $\mathcal{I}_h^k$:
  $\mathcal{A}_{a,h}^k = \{\sigma_h^k - \gamma(u_{a,h}^k - u_h^k) < 0\}$, $\mathcal{A}_{b,h}^k = \{\sigma_h^k + \gamma(u_h^k - u_{b,h}^k) > 0\}$,
  $\mathcal{I}_h^k = \mathbf{1}\backslash\{\mathcal{A}_{a,h}^k \cup \mathcal{A}_{b,h}^k\}$.
  if $\mathcal{A}_{a,h}^k = \mathcal{A}_{a,h}^{k+1}$, $\mathcal{A}_{b,h}^k = \mathcal{A}_{b,h}^{k+1}$, and $\mathcal{I}_h^k = \mathcal{I}_h^{k+1}$ **then**
    STOP.
  end if
  Set $k := k + 1$.
end for

4.2. Optimization algorithm

Algorithm 2 describes the primal-dual active set (PDAS) strategy as a semi-smooth Newton step, see, e.g., [61]. In the procedure, we solve the following discrete linear system:

$$\mathcal{K} = \begin{pmatrix} \mathcal{N}_1 & \cdot & \mathcal{A}_a & \cdot & \cdot \\ \cdot & \omega\mathcal{M}_B & \mathcal{N}_2 & \mathcal{M}_B & \mathcal{M}_B \\ \mathcal{A}_s & \mathcal{N}_3 & \cdot & \cdot & \\ \cdot & \omega\chi_{\mathcal{A}_{b,h}} & \cdot & \chi_{I_h} & \cdot \\ \cdot & \omega\chi_{\mathcal{A}_{a,h}} & \cdot & \cdot & -\chi_{I_h} \end{pmatrix} \begin{pmatrix} \mathcal{Z}_h \\ u_h \\ \mathcal{Y}_h \\ \sigma_h^b \\ \sigma_h^a \end{pmatrix} = \begin{pmatrix} \mathcal{F}_a \\ \cdot \\ \mathcal{F}_s \\ \omega\chi_{\mathcal{A}_{b,h}} u_h^b \\ \omega\chi_{\mathcal{A}_{a,h}} u_h^a \end{pmatrix}, \tag{50}$$

where

$$\mathcal{N}_1 = \begin{pmatrix} \cdot & \cdot & \cdot \\ \cdot & \cdot & \cdot \\ \cdot & \cdot & -\mathcal{M} \end{pmatrix}, \quad \mathcal{N}_2 = \begin{pmatrix} \mathcal{M}_{B1} \\ \mathcal{M}_{B2} \\ \cdot \end{pmatrix}^T, \quad \mathcal{N}_3 = \begin{pmatrix} -\mathcal{M}_{B1} \\ -\mathcal{M}_{B2} \\ \mathcal{SD} + \mathcal{M}_{BC} \end{pmatrix},$$
$$\mathcal{Y}_h = \begin{pmatrix} \mathbf{q}_h \\ y_h \end{pmatrix}, \quad \mathcal{Z}_h = \begin{pmatrix} \mathbf{p}_h \\ z_h \end{pmatrix}.$$

The mass matrices $\mathcal{M}$ and $\mathcal{M}_B$ on the domain and boundary are defined by

$$\mathcal{M}_{ij} = \int_K \varphi_j \varphi_i \, dx, \quad (\mathcal{M}_B)_{ij} = \int_{\partial K} \varphi_j \varphi_i \, dx,$$

respectively. For all $E \in \mathcal{E}^{\partial}$, the variants of mass matrices are given by

$$(\mathcal{M}_{B1})_{ij} = \int_E \epsilon^{\frac{1}{2}} n_1 \, \varphi_j \varphi_i \, ds, \quad (\mathcal{M}_{B2})_{ij} = \int_E \epsilon^{\frac{1}{2}} n_2 \, \varphi_j \varphi_i \, ds,$$
$$(\mathcal{M}_{BC})_{ij} = \int_{E^-} |\beta \cdot \mathbf{n}| \, \varphi_j \varphi_i \, ds, \quad \mathcal{SD}_{ij} = \int_E \frac{\epsilon^{\frac{1}{2}}}{h_E} \varphi_j \varphi_i \, ds,$$

where $\mathbf{n} = (n_1, n_2)^T$ and E^- denotes the inflow boundary.

$\chi_{\mathcal{A}_{a,h}}$, $\chi_{\mathcal{A}_{b,h}}$, and $\chi_{\mathcal{I}_h}$ denote the characteristic functions of $\mathcal{A}_{a,h}$, $\mathcal{A}_{b,h}$, and $\mathcal{I}_h$, respectively, defined on the boundary $\mathcal{E}_h^{\partial}$. The bi-(linear) forms of the state system in (17a)–(17b) are represented by $\mathcal{A}_s$ and $\mathcal{F}_s$, whereas $\mathcal{A}_a$ and $\mathcal{F}_a$ correspond to the bilinear forms of the adjoint system in (17c)–(17d).

4.3. Numerical results

We now present several numerical results in order to examine the quality of derived estimators in Section 3 and the performance of the adaptive loop introduced in Section 4.1. We use piecewise linear polynomials for the approximation of the state, the adjoint, the control, and the Lagrange multipliers. The effectivity index is computed according to

$$\text{effectivity index} = \frac{\eta_h}{|J(y,u) - J_h(y_h - u_h)|}, \tag{51}$$

where η_h consists of the approximations of the primal-dual residuals, the primal-dual mismatch in complementary, and the data oscillations.

In our numerical experiments, the corresponding error estimators are denoted by superscript "A" for adaptive refinement and "U" for uniform refinement. For instance, J_h^A represents the value of the objective function computed on the adaptively refined mesh, whereas J_h^U is the value of the objective function computed on the uniformly refined mesh. Moreover, since we have no explicit expression of the analytic solution in our numerical examples, the solutions y^*, u^* obtained on adaptively refined fine meshes are taken as a reference solutions. Then, the value of the reference objective solution is denoted by $J^* := J(y^*, u^*)$, computed exactly from the solutions y^*, u^*.

4.3.1. Example 1

Our first example defined in the unit square $\Omega = [0,1] \times [0,1]$ has been adopted from [31]. The rest of the data are

$$f = 0, \quad y^d = \frac{1}{(x_1^2 + x_2^2)^{1/3}}, \quad \beta = (1,1)^T, \quad \alpha = 1, \quad \omega = 1.$$

The control set is given by

$$U^{ad} = \{u \in L^2(\Gamma) : \quad -0.75 \le u(x) \le 0 \ \text{ a.e. } x \in \Gamma\}.$$

We have no explicit expression of the analytic solution, therefore we solve the problem numerically for $\epsilon = 10^{-1}$ using 11.374 vertices and 19.043 elements, and then obtained solutions y^*, u^* are used as a reference solution to make a comparison with others. The value of the reference objective function for $\epsilon = 10^{-1}$ is $J(y^*, u^*) = 5.646$. We note that it is a difficult task to determine J^* as accurate as possible. Therefore, the errors and the effectivity indices should be treated with care.

Fig. 1 displays the performance of the error estimator proposed in Section 3 in terms of the number of vertices for the marking parameter $\theta = 0.65$ and the diffusion parameter $\epsilon = 10^{-1}$ on adaptively and uniformly refined meshes. The left plot shows the convergence of $J_h^A - J^*$ on the adapted meshes compared to the convergence of $J_h^U - J^*$ on the uniform meshes. One can observe a reduction of complexity for a certain accuracy in the objective value. The middle plot displays the comparison of convergence of the error estimators as a function of the number of vertices in logarithmic scale for adaptive versus uniform refinement. Last, the right plot exhibits the actual sizes of the state, adjoint, data oscillation, and complementary components of the error estimator. The refinement process is dominated by the contribution of the data oscillations. All parts of the estimators converge to zero, and the estimated error η_h^A on adapted meshes is smaller compared to the ones on uniform meshes.

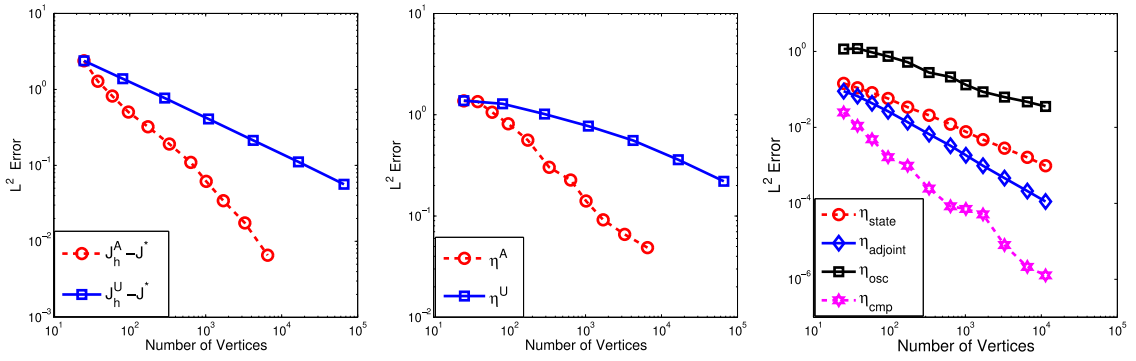

Fig. 1. Section 4.3.1: Convergence of the estimators computed on adaptively and uniformly refined meshes with $\epsilon = 10^{-1}$ and $\theta = 0.65$.

Table 1
Section 4.3.1: Convergence history for $\epsilon = 10^{-1}$ and $\theta = 0.65$ on adaptively refined meshes.

vertices (N)	η_h^A	order	$J_h^A - J^*$	Eff. Ind.
25	1.37e+00	–	2.38e+00	0.58
38	1.35e+00	0.04	1.28e+00	1.05
59	1.06e+00	0.55	8.18e−01	1.29
96	8.14e−01	0.54	5.04e−01	1.62
174	5.61e−01	0.62	3.22e−01	1.74
333	3.03e−01	0.95	1.91e−01	1.59
637	2.27e−01	0.44	1.09e−01	2.07
1016	1.41e−01	1.02	6.15e−02	2.28
1707	9.17e−02	0.82	3.43e−02	2.68
3272	6.59e−02	0.51	1.74e−02	3.78
6538	4.94e−02	0.42	6.50e−03	7.59

Table 2
Section 4.3.1: Convergence history for $\epsilon = 10^{-1}$ on uniformly refined meshes.

# vertices (N)	η_h^U	order	$J_h^U - J^*$	Eff. Ind.
25	1.37e+00	–	2.38e+00	0.58
89	1.28e+00	0.06	1.38e+00	0.93
289	1.02e+00	0.18	7.70e−01	1.32
1089	7.73e−01	0.21	4.08e−01	1.89
4225	5.58e−01	0.24	2.13e−01	2.61
16641	3.60e−01	0.32	1.11e−01	3.24

Convergence history for $\epsilon = 10^{-1}$ on adaptively and uniformly refined meshes are exhibited in Tables 1 and 2, respectively. Despite oscillations, the reduction of estimators η_h^A is close to $N^{-1/2}$, which is the optimal rate we can expect with linear elements. Generally, it is expected that the effectivity index should be close to one however for our example the value of effectivity index is increasing as we refine the mesh. Computation of the reference solution or approximation of the dual solution in the estimator can be reason of this case. However, the results in Table 1 show that the estimator η_h^A becomes reliable.

Fig. 2 shows computed solutions of the control for various values of the diffusion parameter ϵ. As expected, the control constraints are satisfied even for convection dominated case. Last, the adaptively generated meshes are depicted in Fig. 3.

4.3.2. Example 2

Our second example, modified from [34], is defined in a polygonal domain with maximum interior angle $\theta = \frac{5}{6}\pi$ as shown in Fig. 4. The remaining data of the problem are given by

$$y^d = \begin{cases} -1, & 0 \le x_2 < 0.5, \\ 1, & 0.5 \le x_2 < 1, \end{cases} \qquad f = 1, \quad \beta = (2,0)^T, \quad \alpha = 1, \quad \omega = 1.$$

We choose the control set as

$$U^{ad} = \{u \in L^2(\Gamma) : \ \ 0 \le u(x) \le 0.5 \ \ \text{a.e.}\ x \in \Gamma\}.$$

As previous example, an analytical representation is not known. As a substitute for the exact solution of the case $\epsilon = 10^{-1}$, we have chosen the computed solution with respect to a sufficiently fine simplicial triangulation of the

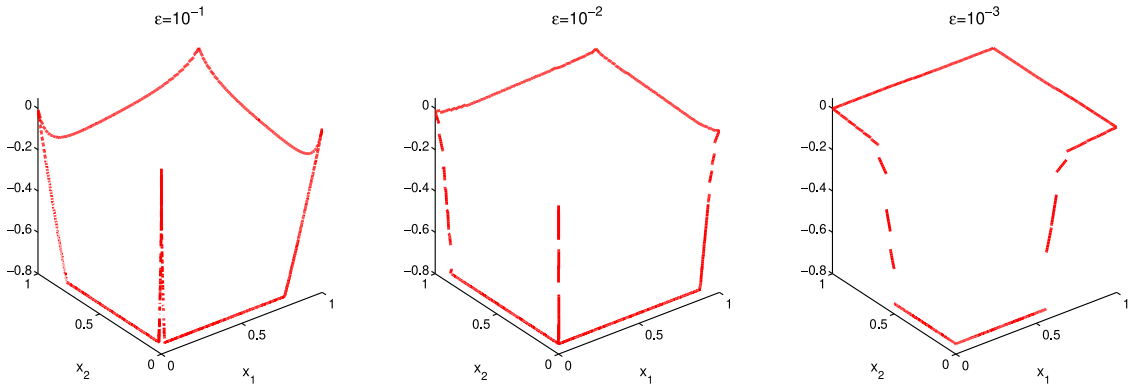

Fig. 2. Section 4.3.1: Computed solutions of the control for different values of $\epsilon = 10^{-1}, 10^{-2}$, and 10^{-3} (from left to right).

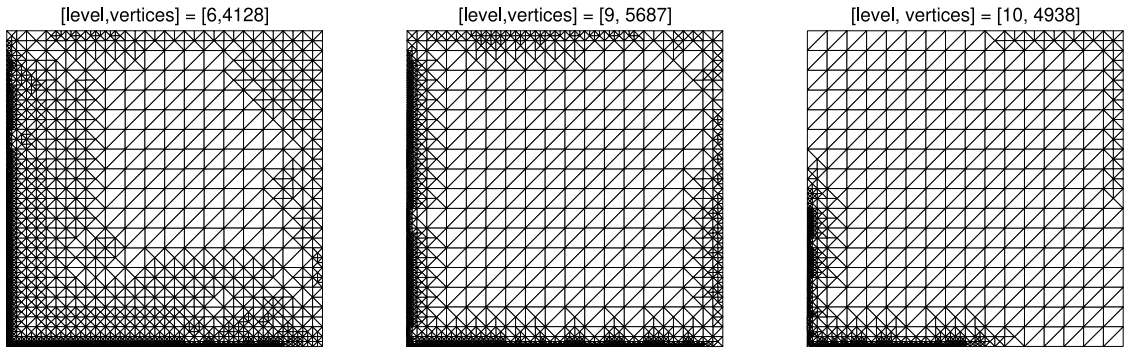

Fig. 3. Section 4.3.1: Adaptively generated meshes for various values of $\epsilon = 10^{-1}, 10^{-2}, 10^{-3}$ with the marking parameter $\theta = 0.8$ (from left to right).

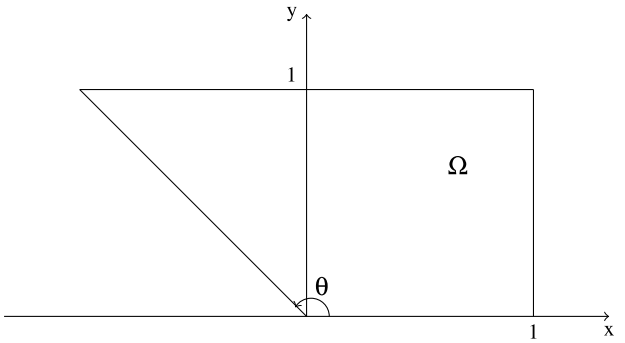

Fig. 4. Section 4.3.2: Domain with $\theta = \frac{5}{6}\pi$.

computational domain with 8.707 vertices and 15.389 elements obtained by adaptive refinement, see Fig. 5 for the corresponding discrete solutions. The value of reference objective function is $J^* = 2.445$.

In Fig. 6, we show the convergence comparison in the quantity of interest (objective functional) $J_h - J^*$ on the adapted meshes and on the uniform meshes (left), the convergence of the error estimator in adaptive versus uniform refinement (middle), and the actual sizes of the state, adjoint, data oscillation, and complementary components of the error estimator (right). As previous example, the error estimator on adaptively refined meshes exhibits a better convergence. Although the complementary component of the estimator converges to zero, it does not decrease monotonically as the other terms of the estimator.

In Table 3, we observe that η_h^A provides an upper bound for the absolute error in the objective function. Reduction of the estimator is around the optimal rate $N^{-1/2}$, where N is the number of vertices. Moreover, convergence history on uniformly refined meshes is exhibited in Table 4.

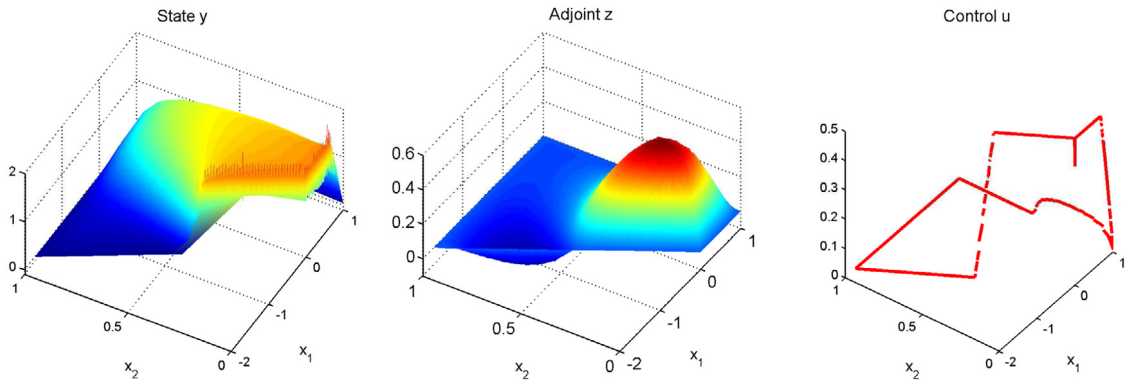

Fig. 5. Section 4.3.2: Computed solutions of the state, adjoint, and control for $\epsilon = 10^{-1}$.

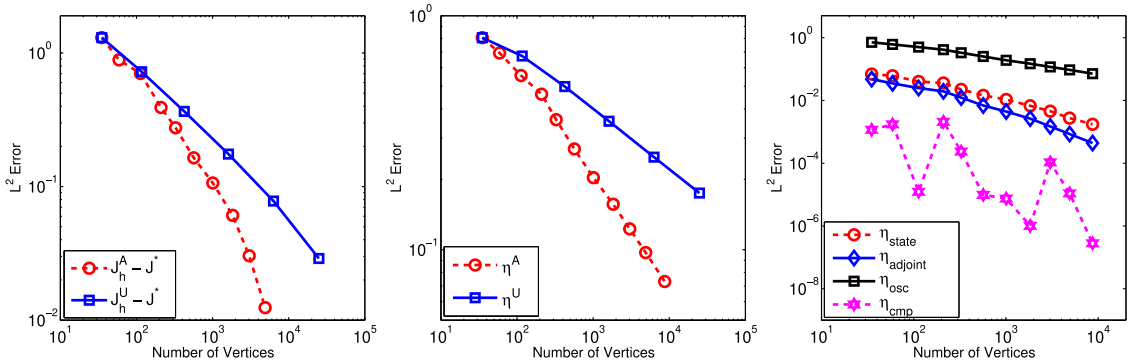

Fig. 6. Section 4.3.2: Comparison of convergence of the estimators on adaptive and uniform refined meshes for $\epsilon = 10^{-1}$ and $\theta = 0.65$.

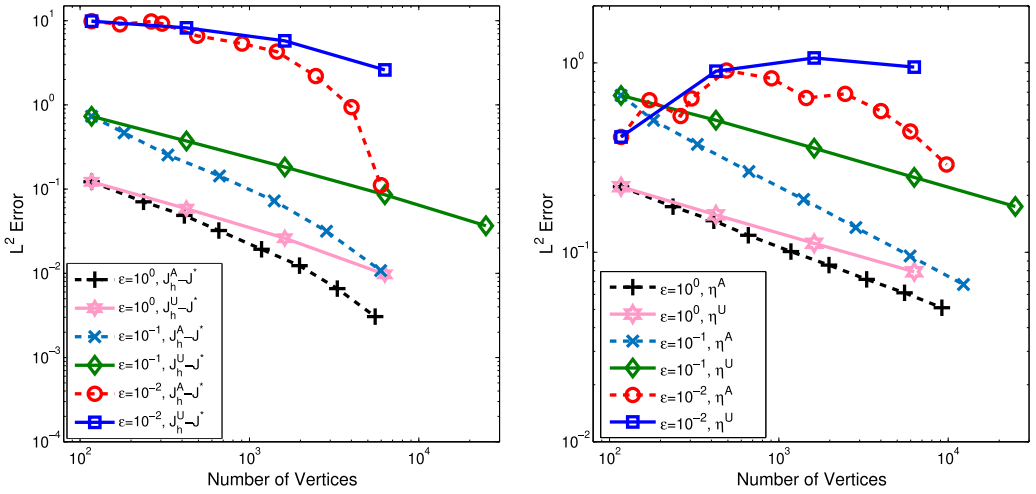

Fig. 7. Section 4.3.2: Comparison of convergence of the estimators on adapted and uniform meshes with different values of $\epsilon = 10^{0}, 10^{-1}$, and 10^{-2} and the marking parameter $\theta = 0.75$.

We next have a closer look at the convergence of $J_h - J^*$ and the estimator η. Fig. 7 illustrates the behaviour of our estimator for different values of the diffusion parameter $\epsilon = 10^{0}, 10^{-1}$, and 10^{-2} on adaptively and uniformly refined meshes with the marking parameter $\theta = 0.75$. After a few steps, the adaptive refinements lead to better convergence than the uniform refinements for all cases.

Table 3
Section 4.3.2: Convergence history of the adaptive method for $\epsilon = 10^{-1}$ and $\theta = 0.65$.

# vertices	η_h^A	order	$J_h^A - J^*$	Eff. Ind.
35	8.06e−01	–	1.30e+00	0.62
59	6.93e−01	0.29	8.88e−01	0.78
113	5.55e−01	0.34	7.02e−01	0.79
210	4.62e−01	0.30	3.90e−01	1.18
327	3.60e−01	0.57	2.75e−01	1.31
567	2.70e−01	0.52	1.64e−01	1.64
1006	2.03e−01	0.49	1.06e−01	1.91
1833	1.56e−01	0.44	6.09e−02	2.57
3023	1.23e−01	0.48	3.04e−02	4.04
4904	9.71e−02	0.48	1.24e−02	7.84

Table 4
Section 4.3.2: Convergence history for $\epsilon = 10^{-1}$ on uniformly refined meshes.

# vertices (N)	η_h^U	order	$J_h^U - J^*$	Eff. Ind.
35	8.06e−01	–	1.30e+00	0.62
117	6.73e−01	0.15	7.24e−01	0.92
425	4.98e−01	0.23	3.65e−01	1.36
1617	3.54e−01	0.25	1.75e−01	2.03
6305	2.49e−01	0.26	7.79e−02	3.19

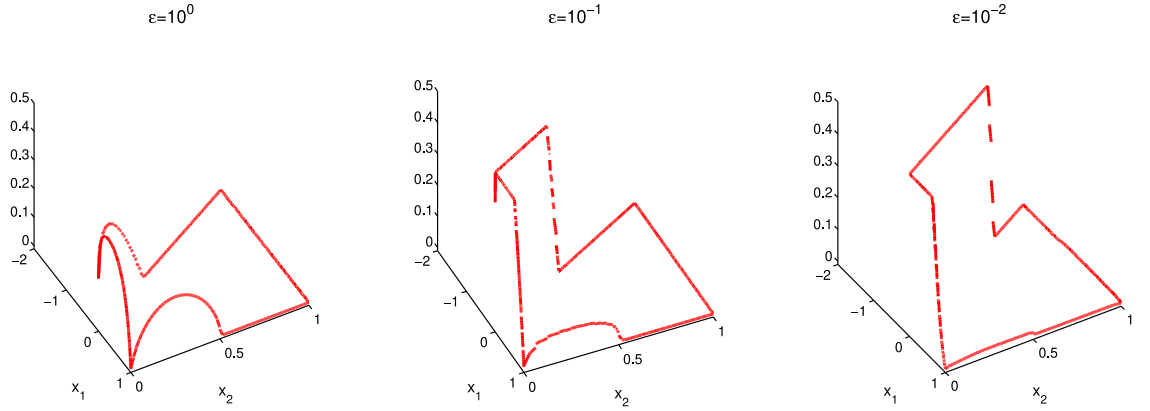

Fig. 8. Section 4.3.2: Computed solutions of the control for different values of $\epsilon = 10^0$, 10^{-1}, and 10^{-2} (from left to right).

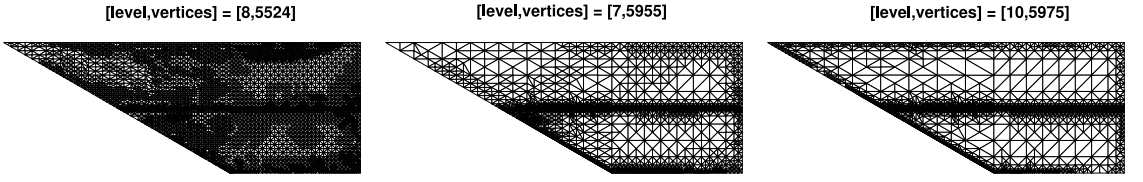

Fig. 9. Section 4.3.2: Adaptively generated meshes for various values of $\epsilon = 10^0$, 10^{-1}, and 10^{-2} with the marking parameter $\theta = 0.75$.

Fig. 8 displays the discrete control solutions for different values of the ϵ. Finally, the adaptively generated meshes for various value of the diffusion parameter ϵ are depicted in Fig. 9. These meshes clearly show that the largest errors in the numerical approximation occur on the boundaries and along $x_2 = 0.5$ and on the boundary of the domain.

5. Conclusions

In this paper, we have studied goal-oriented a posteriori error estimates of local discontinuous Galerkin method for the numerical approximation of Dirichlet boundary control problem governed by a convection diffusion equation with bilateral control constraints. We derive primal-dual weighted error estimates for the objective functional with an error term representing the mismatch in the complementary system due to the discretization. The numerical results show that the adaptive refinements are superior to uniform refinements. We have obtained a reduction of complexity for a certain

accuracy in the objective value and have derived reliable error estimator. Future work will include the extension of our results to Dirichlet boundary optimal control problems with state constraint conditions.

Acknowledgments

The author would like to express his sincere thanks to the anonymous referees for their most valuable suggestions.

References

[1] L. Dedè, S. Micheletti, S. Perotto, Anisotropic error control for environmental applications, Appl. Numer. Math. 58 (9) (2008) 1320–1339.
[2] B. Mohammadi, O. Pironneau, Applied Shape Optimization for Fluids, Oxford University Press, Oxford, 2001.
[3] J. Zhu, Q.C. Zeng, A mathematical formulation for optimal control of air pollution, Sci. China Ser. D Earth Sci. 46 (2003) 994–1002.
[4] I. Babuška, W.C. Rheinboldt, Error estimates for adaptive finite element computations, SIAM J. Numer. Anal. 15 (1978) 736–754.
[5] M. Hintermüller, R.H.W. Hoppe, Y. Iliash, M. Kieweg, An a posteriori error analysis of adaptive finite element methods for distributed elliptic control problems with control constraints, ESAIM Control Optim. Calc. Var. 14 (3) (2008) 540–560.
[6] M. Hinze, N. Yan, Z. Zhou, Variational discretization for optimal control governed by convection dominated diffusion equations, J. Comput. Math. 27 (2–3) (2009) 237–253.
[7] R.H.W. Hoppe, Y. Iliash, C. Iyyunni, N.H. Sweilam, A posteriori error estimates for adaptive finite element discretizations of boundary control problems, J. Numer. Math. 14 (1) (2006) 57–82.
[8] R.H.W. Hoppe, M. Kieweg, Adaptive finite element methods for mixed control-state constrained optimal control problems for elliptic boundary value problems, Comput. Optim. Appl. 46 (3) (2010) 511–533.
[9] R. Li, W. Liu, H. Ma, T. Tang, Adaptive finite element approximation for distributed elliptic optimal control problems, SIAM J. Control Optim. 41 (5) (2002) 1321–1349.
[10] W. Liu, N. Yan, A posteriori error estimates for distributed convex optimal control problems, Adv. Comput. Math. 15 (2001) 285–309.
[11] N. Yan, Z. Zhou, A priori and a posteriori error analysis of edge stabilization Galerkin method for the optimal control problem governed by convection-dominated diffusion equation, J. Comput. Appl. Math. 223 (1) (2009) 198–217.
[12] H. Yücel, P. Benner, Adaptive discontinuous Galerkin methods for state constrained optimal control problems governed by convection diffusion equations, Comput. Optim. Appl. 62 (2015) 291–321.
[13] H. Yücel, B. Karasözen, Adaptive symmetric interior penalty Galerkin (SIPG) method for optimal control of convection diffusion equations with control constraints, Optimization 63 (2014) 145–166.
[14] Z. Zhou, X. Yu, N. Yan, The local discontinuous Galerkin approximation of convection-dominated diffusion optimal control problems with control constraints, Numer. Methods Partial Differential Equations 30 (1) (2014) 339–360.
[15] J. Oden, S. Prudhomme, Goal-oriented error estimation and adaptivity for the finite element method, Comput. Math. Appl. 41 (5) (2001) 735–756.
[16] E. Rabizadeh, A.S. Bagherzadeh, T. Rabczuk, Adaptive thermo-mechanical finite element formulation based on goal-oriented error estimation, Comput. Mater. Sci. 102 (2015) 27–44.
[17] E. Rabizadeh, A.S. Bagherzadeh, T. Rabczuk, Goal-oriented error estimation and adaptive mesh refinement in dynamic coupled thermoelasticity, Comput. Struct. 173 (2016) 187–211.
[18] R. Becker, H. Kapp, R. Rannacher, Adaptive finite element methods for optimal control of partial differential equations: Basic concepts, SIAM J. Control Optim. 39 (2000) 113–132.
[19] M. Hintermüller, R.H.W. Hoppe, Goal-oriented adaptivity in control constrained optimal control of partial differential equations, SIAM J. Control Optim. 47 (4) (2008) 1721–1743.
[20] B. Vexler, W. Wollner, Adaptive finite elements for elliptic optimization problems with control constraints, SIAM J. Control Optim. 47 (2008) 509–534.
[21] O. Benedix, B. Vexler, A posteriori error estimation and adaptivity for elliptic optimal control problems with state constraints, Comput. Optim. Appl. 44 (1) (2009) 3–25.
[22] A. Günther, M. Hinze, A posteriori error control of a state constrained elliptic control problem, J. Numer. Math. 16 (2008) 307–322.
[23] M. Hintermüller, R.H.W. Hoppe, Goal-oriented adaptivity in pointwise state constrained optimal control of partial differential equations, SIAM J. Control Optim. 48 (2010) 5468–5487.
[24] W. Wollner, A posteriori error estimates for a finite element discretization of interior point methods for an elliptic optimization problem with state constraints, Comput. Optim. Appl. 47 (1) (2010) 133–159.
[25] W. Bangerth, M. Geiger, R. Rannacher, Adaptive Galerkin finite element methods for the wave equation, Comput. Methods Appl. Math. 10 (2010) 3–48.
[26] W. Bangerth, R. Rannacher, Adaptive Finite Element Methods for Differential Equations, in: Lectures in Mathematics, ETH Zürich, Birkhäuser Verlag, Basel, 2003.
[27] M. Schmich, B. Vexler, Adaptivity with dynamic meshes for space–time finite element discretizations of parabolic equations, SIAM J. Sci. Comput. 30 (2008) 369–393.
[28] J.-L. Lions, Optimal Control of Systems Governed By Partial Differential Equations, Springer, Berlin, 1971.
[29] F. Tröltzsch, Optimal Control of Partial Differential Equations: Theory, Methods and Applications, in: Graduate Studies in Mathematics, vol. 112, American Mathematical Society, Providence, RI, 2010.
[30] M. Berggren, Approximations of very weak solutions to boundary-value problems, SIAM J. Numer. Anal. 42 (2) (2004) 860–877.
[31] E. Casas, J.-P. Raymond, Error estimates for the numerical approximation of Dirichlet boundary control for semilinear elliptic equations, SIAM J. Control Optim. 45 (5) (2006) 1586–1611.
[32] K. Deckelnick, A. Günther, M. Hinze, Finite element approximation of Dirichlet boundary control for elliptic PDEs on two–and three–dimensional curved domains, SIAM J. Control Optim. 48 (2009) 2798–2819.
[33] M. Mateos, Optimization methods for Dirichlet control problems, Optimization 67 (2018) 585–617.
[34] S. May, R. Rannacher, B. Vexler, Error analysis for a finite element approximation of elliptic Dirichlet boundary control problems, SIAM J. Control Optim. 51 (2013) 2585–2611.
[35] T. Apel, M. Mateos, J. Pfefferer, A. Rösch, On the regularity of the solutions of Dirichlet optimal control problems in polygonal domains, SIAM J. Control Optim. 53 (6) (2015) 3620–3641.
[36] S. Chowdhury, T. Gudi, A.K. Nandakumaran, Error bounds for a Dirichlet boundary control problem based on energy spaces, Math. Comp. 86 (2017) 1103–1126.

[37] W. Gong, W. Liu, Z. Tan, N. Yan, A convergent adaptive finite element method for elliptic Dirichlet boundary control problems, IMA J. Numer. Anal. 39 (4) (2019) 1985–2015.
[38] G. Of, T.X. Phan, O. Steinbach, An energy space finite element approach for elliptic Dirichlet boundary control problems, Numer. Math. 129 (4) (2015) 723–748.
[39] F. Belgacem, H.E. Fekih, H. Metoui, Singular perturbation for the Dirichlet boundary control of elliptic problems, M2AN Math. Model. Numer. Anal. 37 (2003) 850–883.
[40] W. Gong, N. Yan, Mixed finite element method for Dirichlet boundary control problem governed by elliptic PDEs, SIAM J. Control Optim. 49 (3) (2011) 984–1014.
[41] D.N. Arnold, F. Brezzi, B. Cockburn, L.D. Marini, Unified analysis of discontinuous Galerkin methods for elliptic problems, SIAM J. Numer. Anal. 39 (5) (2002) 1749–1779.
[42] B. Cockburn, Devising discontinuous Galerkin methods for non-linear hyperbolic conservation laws, J. Comput. Phys. 128 (2001) 187–204.
[43] B. Rivière, Discontinuous Galerkin Methods for Solving Elliptic and Parabolic Equations. Theory and Implementation, in: Frontiers Appl. Math., SIAM, Philadelphia, 2008.
[44] P. Benner, H. Yücel, Adaptive symmetric interior penalty Galerkin method for boundary control problems, SIAM J. Numer. Anal. 55 (2) (2017) 1101–1133.
[45] D. Leykekhman, M. Heinkenschloss, Local error analysis of discontinuous Galerkin methods for advection-dominated elliptic linear-quadratic optimal control problems, SIAM J. Numer. Anal. 50 (4) (2012) 2012–2038.
[46] H. Yücel, M. Heinkenschloss, B. Karasözen, Distributed Optimal Control of Diffusion-Convection-Reaction Equations using Discontinuous Galerkin Methods, in: Numer. Math. Adv. Appl., vol. 2011, Springer, Berlin, 2013, pp. 389–397.
[47] P. Benner, H. Yücel, A Local Discontinuous Galerkin Method for Dirichlet Boundary Control Problems, Tech. Rep., 2018.
[48] W. Gong, W. Hu, M. Mateos, J. Singler, X. Zhang, Y. Zhang, A new HDG method for Dirichlet boundary control of convection diffusion PDEs II: Low regularity, SIAM J. Numer. Anal. 56 (4) (2018) 2262–2287.
[49] W. Hu, M. Mateos, J. Singler, Y. Zhang, A New HDG Method for Dirichlet Boundary Control of Convection Diffusion PDEs I: High Regularity, Tech. Rep., 2018, arXiv:1801.01461v1.
[50] K. Kunisch, B. Vexler, Constrained Dirichlet boundary control in L^2 for a class of evolution equations, SIAM J. Control Optim. 46 (5) (2007) 1726–1753.
[51] B. Vexler, Finite element approximation of elliptic Dirichlet optimal control problems, Numer. Funct. Anal. Optim. 28 (7–8) (2007) 957–973.
[52] P.G. Ciarlet, The Finite Element Method for Elliptic Problems, North–Holland, Amsterdam, New York, 1978.
[53] P. Castillo, B. Cockburn, I. Pergugia, D. Schötzau, An a priori error analysis of the local discontinuous Galkerin method for elliptic problems, SIAM J. Numer. Anal. 38 (2000) 1676–1706.
[54] M. Hintermüller, K. Ito, K. Kunisch, The primal–dual active set strategy as a semismooth Newton method, SIAM J. Optim. 13 (3) (2003) 865–888.
[55] R. Griesse, S. Volkwein, A primal–dual active set strategy for optimal boundary control of a nonlinear reaction–diffusion system, SIAM J. Control Optim. 44 (2) (2005) 467–494.
[56] R. Becker, R. Rannacher, An optimal control approach to a posteriori error estimation in finite element methods, Acta Numer. 10 (2001) 1–102.
[57] F. Brezzi, M. Fortin, Mixed and Hybrid Finite Element Methods, in: Computational Mathematics, vol. 15, Springer, Berlin, 1991.
[58] Y. Chen, W. Liu, Error estimates and superconvergence of mixed finite element for quadratic optimal control, Int. J. Numer. Anal. Model. 3 (2006) 311–321.
[59] L. Angermann, C. Henke, Interpolation, projection and hierarchical bases in discontinuous Galerkin methods, Numer. Math. Theory Methods Appl. 8 (3) (2015) 425–450.
[60] S.C. Brenner, L.R. Scott, The Mathematical Theory of Finite Element Methods, third ed., Springer, Berlin, 2008.
[61] M. Bergounioux, K. Ito, K. Kunisch, Primal–dual strategy for constrained optimal control problems, SIAM J. Control Optim. 37 (4) (1999) 1176–1194.